Time- and size-resolved chemical composition of submicron particles in Pittsburgh: Implications for aerosol sources and processes

Qi Zhang
Cooperative Institute for Research in Environmental Sciences, University of Colorado, Boulder, Colorado, USA

Manjula R. Canagaratna, John T. Jayne, and Douglas R. Worsnop
Aerodyne Research Inc., Billerica, Massachusetts, USA

Jose-Luis Jimenez
Cooperative Institute for Research in Environmental Sciences, University of Colorado, Boulder, Colorado, USA

Department of Chemistry and Biochemistry, University of Colorado, Boulder, Colorado, USA

Received 15 February 2004; revised 4 August 2004; accepted 11 August 2004; published 25 January 2005.

[1] An Aerodyne aerosol mass spectrometer (AMS) was deployed at the Pittsburgh Environmental Protection Agency Supersite from 7 to 22 September 2002 as part of the Pittsburgh Air Quality Study (PAQS). The main objectives of this deployment were to characterize the concentrations, size distributions, and temporal variations of nonrefractory (NR) chemical species in submicron particles (approximately PM_1) and to further develop and evaluate the AMS. Reasonably good agreement was observed on particle concentrations, composition, and size distributions between the AMS data and measurements from collocated instruments (given the difference between the PM_1 and $PM_{2.5}$ size cuts), including TEOM, semicontinuous sulfate, 2-hour- and 24-hour-averaged organic carbon, SMPS, 4-hour-averaged ammonium, and micro-orifice uniform deposit impactor. Total NR-PM_1 mass concentration in Pittsburgh accumulates over periods of several days punctuated with rapid cleaning due to rain or air mass changes. Sulfate and organics are the major NR-PM_1 components while the concentrations of nitrate and chloride are generally low. Significant amounts of ammonium, which most of the time are consistent with sulfate present as ammonium sulfate, are also present in particles. However, there are periods when the aerosols are relatively acidic and more than 50% of sulfate is estimated to be in the form of ammonium bisulfate. No major enhancement of the organic concentration is observed during these acidic periods, which suggests that acid-catalyzed SOA formation was not an important process during this study. Size distributions of particulate sulfate, ammonium, organics, and nitrate vary on timescales of hours to days, showing unimodal, bimodal and even trimodal characteristics. The accumulation mode (peaking around 350–600 nm in vacuum aerodynamic diameter for the mass distributions) and the ultrafine mode (<100 nm) are observed most frequently. The accumulation mode is dominated by sulfate that appears to be internally mixed with oxidized organics, while combustion-emitted organics are often the main component of the ultrafine particles (except during nucleation events). The ultrafine-mode organic aerosols are mainly associated with combustion sources (likely traffic).

Citation: Zhang, Q., M. R. Canagaratna, J. T. Jayne, D. R. Worsnop, and J.-L. Jimenez (2005), Time- and size-resolved chemical composition of submicron particles in Pittsburgh: Implications for aerosol sources and processes, *J. Geophys. Res.*, *110*, D07S09, doi:10.1029/2004JD004649.

1. Introduction

[2] Atmospheric aerosols have important adverse impacts on human health [*Dockery et al.*, 1993; *Pope et al.*, 2002], visibility [*Watson*, 2002], and ecological integrity [*Bytnerowicz and Fenn*, 1996; *Paerl et al.*, 1997; *Schindler*, 1988]. Aerosols also play important roles in atmospheric processes that are intrinsically linked to climate change [*Intergovernmental Panel on Climate Change* (*IPCC*), 2001] and stratospheric ozone depletion [*Solomon*, 1999]. While a thorough understanding of particle concentration, size distribution, chemical composition, state of mixing, and morphology is essential to address the radiative, ecological and human health effects of atmospheric particles, our knowledge of these parameters is usually limited by the

0148-0227/05/2004JD004649$09.00

coarse time and size resolution of most existing instrumentation for aerosol chemical measurements [*McMurry*, 2000].

[3] Several instruments that are capable of performing real-time and continuous (or semicontinuous) size-resolved measurement of ambient aerosol composition have been developed in the last decade [*Jayne et al.*, 2000; *Murphy et al.*, 1998; *Suess and Prather*, 1999]. Compared to the traditional multistage impactor technologies, online techniques are usually faster, less labor intensive, and less vulnerable to artifacts introduced during sample collection and processing. While most recently developed size-resolved composition instruments measure the qualitative composition of single particles [*Middlebrook et al.*, 2003], the Aerodyne aerosol mass spectrometer (AMS) can determine the sizes and chemical composition of the ensemble of submicron particles in situ, with time resolution of minutes for typical ambient measurements [*Jayne et al.*, 2000; *Jimenez et al.*, 2003c]. The AMS has been successfully employed in more than 30 field campaigns and laboratory studies to characterize the properties, identify the possible sources and elucidate the dynamics of ambient and laboratory aerosols [e.g., *Alfarra et al.*, 2004; *Allan et al.*, 2003a; *Bahreini et al.*, 2003; *Canagaratna et al.*, 2004; *Drewnick et al.*, 2004b; *Jimenez et al.*, 2003b, 2003c; *Morris et al.*, 2002; *Zhang et al.*, 2004].

[4] We deployed an AMS in Pittsburgh, Pennsylvania, during September 2002, as part of the Pittsburgh Air Quality Study (PAQS). PAQS was sponsored by the U.S. Environmental Protection Agency to address the relationship between particulate matter (PM) and health effects, establish the PM source-receptor relationships, and develop and evaluate the next generation of PM monitoring techniques [*Wittig et al.*, 2004]. The focus of this AMS deployment was to characterize the chemistry and dynamics of ambient aerosols with high time and size resolution and therefore offer insights into the sources and processes of particles in the Pittsburgh region. In this paper, we mainly report the size-resolved chemical composition, concentrations, and temporal variations of the nonrefractory particle components (i.e., sulfate, organics, ammonium and nitrate). Quality control measures, such as corrections for nonideality of the AMS measurements and comparisons between the AMS results and various collocated measurements, are also reported. The chemistry and growth mechanisms of ultrafine particles during nucleation events in Pittsburgh [*Zhang et al.*, 2004] and a more detailed organic analysis (Q. Zhang et al., Deconvolution and quantification of primary and oxygenated organic aerosols based on aerosol mass spectrometry: Part 1. Development and validation of the method, submitted to *Environmental Science and Technology*, 2004) (hereinafter referred to as Zhang et al., submitted manuscript, 2004) are discussed in separate papers.

2. Experimental Methods

2.1. Sampling Site and Time

[5] The AMS was operated at the PAQS central site (40°27′N, 79°57′W) continuously, except for occasional maintenance and calibration, from 7 to 22 September 2002. This site was located ~6 km east of downtown Pittsburgh, on a hill of Schenley Park next to Carnegie Mellon University [*Wittig et al.*, 2004]. Baseline monitoring for PM, gas-phase and meteorological variables lasted for ~15 months at this site from July 2001 to October 2002 [*Wittig et al.*, 2004]. An overview of PAQS and the Supersite operation was given by *Wittig et al.* [2004]. Other details can be found in the PAQS Quality Assurance Project Plan prepared by *Khlystov et al.* [2001].

[6] All dates and times are reported in Eastern Standard Time (EST). The local time during this study was Eastern Daylight Saving Time (EDT), which is 1 hour ahead of EST.

2.2. AMS Instrument and Its Operation

2.2.1. Description of the AMS

[7] The AMS has been described in detail in other publications [*Alfarra et al.*, 2004; *Allan et al.*, 2003b; *Jayne et al.*, 2000; *Jimenez et al.*, 2003c]; thus only a brief overview is given here. The AMS consists of three major parts: a particle beam generation inlet system, an aerodynamic sizing chamber, and a particle composition detection section. The inlet system contains a 100 μm critical orifice that sets the airflow into the AMS at a nominal rate of ~1.4 cm^3 s^{-1} and an aerodynamic lens system that focuses particles into a narrow beam of about 100 μm in diameter [*Heberlein et al.*, 2001].

[8] Particles acquire size-dependent velocities upon supersonic expansion into the high-vacuum sizing chamber, where their vacuum aerodynamic diameters (D_{va}) are determined on the basis of calibration using particles of known sizes, densities, and shapes, such as polystyrene latex (PSL) spheres. Details on D_{va} (effectively the aerodynamic diameter measured in the free-molecular regime) and its relationships with mobility diameter (D_m) and the traditional aerodynamic diameter (measured in the continuum regime) are given by *Canagaratna et al.* [2004], *Jimenez et al.* [2003a, 2003b], and *DeCarlo et al.* [2004].

[9] In the composition detection section, particles are flash vaporized upon impact with a heated surface (~600°C during this study) under high vacuum (~10^{-8} torr). The resulting vapor molecules are ionized by electron impact and the positive ions formed are analyzed by a quadrupole mass spectrometer (Balzers QMA410, Balzers, Liechtenstein). Because of the use of thermal vaporization, only nonrefractory (NR) particle components, such as SO_4^{2-}, NO_3^-, NH_4^+ and organics, are determined. "Nonrefractory" is defined operationally as those species that evaporate on timescales of a few seconds (i.e., one period of the blocked/open alternation of the particle beam chopper during the MS mode operation) or less under the AMS conditions. Minerals and elemental carbon are undetectable because of their very low vapor pressure at ~600°C. In addition, since the AMS used in this study has an approximate 1 μm transmission size cut, the results of its measurements are referred to as NR-PM_1.

[10] The AMS alternates between the particle time of flight (P-TOF) mode and the mass spectrum (MS) mode during operation [*Jimenez et al.*, 2003c]. A set of preselected m/z is scanned as a function of particle's time of flight in the P-TOF mode, from which the ensemble size distributions of aerosol species are derived. Mass loadings are calculated from the ensemble background-subtracted mass spectra (m/z 1–300) acquired during the MS mode operation using a software package developed by *Allan et al.*

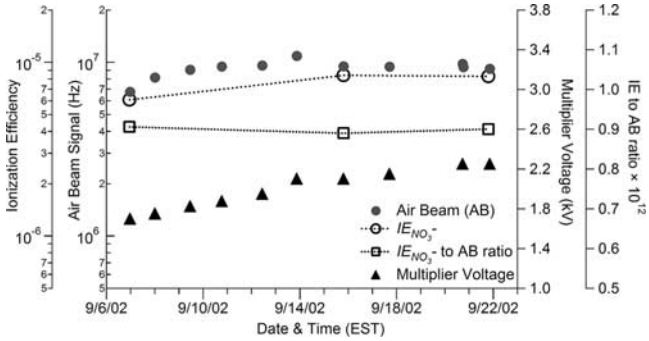

Figure 1. Ionization and ion transmission efficiency for nitrate ($IE_{NO_3^-}$) determined during IE calibrations, multiplier voltage and air beam signal (N_2^+) measured immediately after each EM calibration, and the ratio of $IE_{NO_3^-}$ to air beam signal.

[2004b]. Interferences for the mass concentration and size distribution data are checked according to procedures described by *Jimenez et al.* [2003c] using a data diagnostics module (AMS Diagnostics 1.1.7a) developed by A. Delia (CU).

[11] Note that the AMS used here is not a single particle technique because the quadrupole MS measures only one m/z at any one time, instead of the complete mass spectrum of individual particles. Reported AMS mass spectra and size distributions are the averages over specified intervals (5–10 min for this study; see section 2.2.2).

2.2.2. Operation of the AMS

[12] The AMS, along with a number of other PAQS sampling instruments, was housed in a 33 m^2 trailer during this study [*Wittig et al.*, 2004]. Ambient air was drawn into the AMS through a thermally insulated copper tube (~5 m long and 0.95 cm ID) from ~2 m above the trailer rooftop. Coarse particles were removed using a cyclone with a 2.5 μm cutoff (model URG-2000-30EN, URG, Chapel Hill, North Carolina). The total flow through the copper tube was 10 L min^{-1}, out of which ~0.1 L min^{-1} was isokinetically sampled from the center of the tube by the AMS and the rest was exhausted by the sampling pump. The residence time of sample air in the tube was ~7 s.

[13] The AMS alternated between the P-TOF and MS modes every ~25 s. During the P-TOF mode operation signals of twelve m/z that are representative for NO_3^- (m/z 30 and 46), SO_4^{2-} (m/z 48 and 64), organics (m/z 43, 44, 55, and 57), NH_4^+ (m/z 15 and 16), H_2O (m/z 18), and N_2 (m/z 28) were recorded as a function of particle's time of flight. Four additional (mostly) organic fragments (m/z 27, 67, 91, and 95) were scanned after 8:55 pm on 13 September. Reported mass concentrations and size distributions are the averages over periods of 10 min before 9:50 am on 12 September and 5 min afterward.

2.2.3. Instrument Calibrations

[14] The AMS was calibrated several times for electron multiplier (EM) gain, ionization and ion transmission and detection efficiency (*IE*), and particle sizing during this study (Figure 1). The electron multiplier was calibrated every 1–2 days to compensate for the normal reduction in sensitivity over time and to restore optimum ion signals. *IE*, which is defined as the ratio of ions detected by the multiplier to the number of the parent molecules vaporized in the AMS, was calibrated with monodisperse pure ammonium nitrate particles generated from an aqueous solution by a Collison atomizer (TSI model 3076, St. Paul, Minnesota) and a differential mobility analyzer custom built by Aerodyne Research (using the TSI DMA, model 3081). Monodisperse polystyrene latex spheres (PSL; Duke Scientific, Palo Alto, California) with nominal sizes of 50, 81, 155, 350, 600, and 700 nm and density of 1.054 g cm^{-3} were used to calibrate the AMS sizing. Detailed quantification protocols are described in previous publications [*Alfarra et al.*, 2004; *Allan et al.*, 2003b; *Jayne et al.*, 2000; *Jimenez et al.*, 2003c].

2.3. Quality Assurance and Quality Control (QA/QC)

2.3.1. AMS Detection Efficiency

[15] In order to minimize uncertainties in the reported mass concentrations it is desirable that the fluctuations of the detection efficiency of the AMS are closely monitored and properly corrected throughout the whole campaign. The parameters that capture the AMS detection efficiency are $IE_{NO_3^-}$, which is the ionization efficiency of a reference compound (NO_3^-), and the air beam signal (*AB*), which is the ion rate (Hz) detected for the direct beam of a major air component, e.g., N_2^+ [*Allan et al.*, 2003b; *Jimenez et al.*, 2003c]. While *AB* can be monitored continuously during instrument operation, the determination of $IE_{NO_3^-}$ requires interruption of sampling to perform a calibration experiment (typically 1–2 hours). Given this restriction and the expectation (based on previous experience) that variations in *IE* can be corrected by changes in air beam signal (i.e., the ratio of IE to air beam signal was usually relatively stable) three $IE_{NO_3^-}$ calibrations were conducted during this study (Figure 1). The measured $IE_{NO_3^-}$ values increase by ~50% between the first two calibrations but are constant between the second and the third, suggesting an improvement in the general detection efficiency of the AMS during the first few days of operation. This initial increase in detection efficiency has very often been observed after initial pump-down of the AMS and is possibly due to an enhancement in the detection efficiency (ratio of output signal pulses to ions impacting the first dynode surface) of the electron multiplier detector after its surfaces degas. Because the ratios of $IE_{NO_3^-}$ to *AB* remain remarkably constant during this study (r.s.d. < 1%) the continuous *AB* signal can be used to correct for the variations in the AMS detection efficiencies to a very good approximation.

2.3.2. AMS Collection Efficiency (CE) and Relative Ionization Efficiency (RIE)

[16] CE is introduced to correct for incomplete detection of NR-PM_1 by the AMS [*Alfarra et al.*, 2004], e.g., due to the fact that a fraction of irregularly shaped particles may not reach the AMS vaporizer [*Jayne et al.*, 2000; *Tobias et al.*, 2000] or due to particle bounce from less-volatile particles (T. Onasch, Aerodyne Research, personal communication, 2004). Note that CE accounts only for the fraction of PM_1 that may not be detected by the AMS, and is not intended to account for the difference in size cutoffs between the AMS (approximately PM_1) and $PM_{2.5}$ instruments. The AMS reports PM_1 concentrations and we have made no attempt to predict $PM_{2.5}$ concentrations on the basis of our PM_1 measurement. Although strictly speaking

Table 1. Relative Ionization Efficiencies With Respect to Measured $IE_{NO_3^-}$ and Collection Efficiencies for Individual Species[a]

Chemical Species	RIE	CE
Sulfate	1.15	0.5
Ammonium	3.8[b]	0.5
Organics	1.4	0.7[c]
Nitrate	1.1[d]	0.5

[a]RIE, relative ionization efficiency; CE, collection efficiency.
[b]This value was measured during the IE calibrations in this study.
[c]This value is the weighted average CE of primary and secondary organic aerosols (see section 2.3.2).
[d]$RIE_{NO_3^-}$ = true IE of nitrate/$IE_{NO_3^-}$, where the true IE of nitrate was calculated from all fragments produced by NO_3^- while the $IE_{NO_3^-}$ was determined only on the basis of two major NO_3^- fragments: *m*/*z* 30 and 46.

CE should be a function of particle size, composition, and shape, at present it is defined as the correction factor for the bulk mass concentrations, i.e., the fraction of the particle mass that is measured by the AMS, relative to what would have been measured if all particles were spherical and particle bounce was negligible. In addition, while the component of the AMS collection efficiency due to losses of nonspherical particles can now be measured in real time using a particle beam width probe (BWP) system (J. A. Huffman et al., manuscript in preparation, 2004) this device was not available at the time of this study. We therefore chose CE values on the basis of the general characteristics of the Pittsburgh aerosols and previous experience from multiple field campaigns and laboratory experiments.

[17] A CE value of 0.5 is assigned to sulfate (Table 1), on the basis of observations from several laboratory and field tests for sulfate aerosols [*Alfarra et al.*, 2004; *Allan et al.*, 2004a, 2003b; *Drewnick et al.*, 2004a]. The same CE value (i.e., 0.5) is applied to nitrate and ammonium, because they appear to be internally mixed with sulfate in particles for most of the time in Pittsburgh.

[18] The CE value for total NR-PM_1 organics is estimated on the basis of their size distributions, which often show two modes: a larger accumulation mode that appears to be internally mixed with SO_4^{2-}, NO_3^- and NH_4^+, and a smaller mode that seems to be mainly emitted from combustion sources (see section 3.2.2). A CE value of 0.5 is thus applied to the accumulation mode organics (due to the likely internal mixing with SO_4^{2-}) while CE for the smaller mode is assumed to be 1.0 because a recent laboratory study has shown close to 100% AMS transmission and detection for sooty combustion particles [*Slowik et al.*, 2004]. By studying the size distributions of total organics, as well as individual organic *m*/*z*, averaged over the whole sampling period we found that these two modes can be best separated at D_{va} = 160 nm and that the mass ratio of the smaller (D_{va} < 160 nm) to the larger mode (D_{va} > 160 nm) is roughly 2/3. The CE value of the bulk organics is therefore set at 0.7 (Table 1).

[19] Relative ionization efficiency (RIE) is the ratio of the electron impact ionization efficiency of a given species to $IE_{NO_3^-}$ on a per unit mass basis. RIE values of individual species (Table 1) are determined following the approach described by *Jimenez et al.* [2003c] and *Alfarra et al.* [2004].

[20] Although CE and RIE for organic aerosols in this study are likely to be size dependent, at this point we have chosen to apply constant values (i.e., CE = 0.7 and RIE = 1.4) throughout the whole size range and time period of this study. Going beyond this simple approach requires a technique that can separate the contributions of the various organic aerosol types, and thus allow the application of separate values of CE and RIE to each type. One such technique has recently been developed by our group and is presented in a separate publication (Zhang et al., submitted manuscript, 2004). The direct quantification of the component of CE due to particle shape using the AMS BWP described above (J. A. Huffman et al., manuscript in preparation, 2004), and the use of particle humidification and/or the redesign of the AMS vaporizer to reduce particle bounce will further reduce the uncertainties in mass quantification for future studies.

[21] An important consequence of applying constant CE and RIE is that the proportion of the small mode and accumulation mode in the reported organic size distribution is likely distorted. First, the CE of the accumulation mode organic aerosols is likely smaller than 0.7 while that of the ultrafine mode is likely larger. Also because the average RIE of combustion-emitted organic species is larger than that of oxygenated organics [*Jimenez et al.*, 2003c], RIE of accumulation mode organics is expected to be smaller than 1.4 while that of the ultrafine mode is larger. Thus the small mode, mainly primary organics are likely overestimated, while the accumulation mode, mostly oxygenated organics are likely underestimated.

2.3.3. Detection Limits of the AMS Measurements

[22] The detection limits (DL) of the AMS measurements of mass concentration are evaluated on the basis of the mass spectra of particle free ambient air (filtered with a HEPA filter). The species DLs are defined as 3 times the standard deviation of the corresponding species signals in the filtered air. The DLs of SO_4^{2-}, NH_4^+, NO_3^-, and organics during this study are estimated to be 0.05, 0.11, 0.01, and 0.15 $\mu g\ m^{-3}$, respectively, for a 10 min averaging time (Table 2). Note that these values are 2–3 times higher (i.e., worse) than the 3σ instrumental detection limits defined by *Allan et al.* [2004a, 2004b, 2003b], but 1–2 orders of magnitude lower (i.e., better) than those of the ACE-Asia campaign [*Bahreini et al.*, 2003]. The major reason for the 3σ instrumental DLs estimated by *Allan et al.* [2004a, 2003b] to be smaller is that they only take into account uncertainties due to electronic noise and the ion counting statistics of the background [*Allan et al.*, 2003a, 2003b]. The substantially lower sensitivity of the AMS during the ACE-Asia study was attributed to a relatively high level of background signals in the AMS due to a less optimized vacuum system and inability to

Table 2. Summary of AMS Mass Concentration Data

	Mass Concentration, $\mu g\ m^{-3}$					
	Sulfate	Ammonium	Nitrate	Organics	Chloride	Total
Average	6.95	2.45	0.87	4.48	0.06	14.81
1σ	4.95	1.56	0.94	2.75	0.16	9.01
Median	5.99	2.31	0.56	4.24	0.01	13.75
Minimum	0.17	0.07	0.01	0.17	−0.01	0.56
Maximum	23.92	10.49	13.48	51.17	2.45	70.59
DL[a]	0.05	0.11	0.01	0.15	0.01	0.19

[a]Detection limit at an averaging time of 10 min (see section 2.3.3 for details).

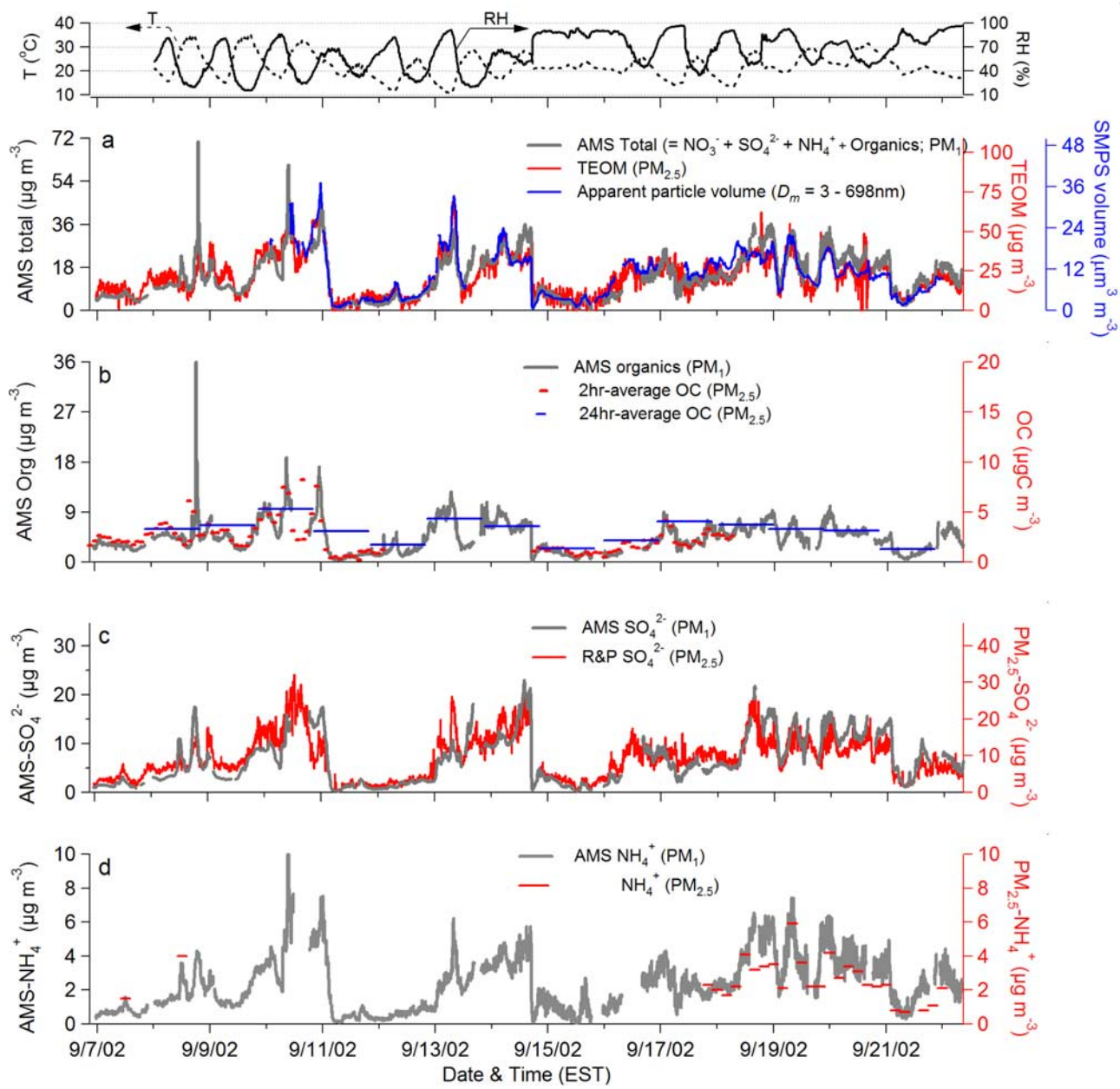

Figure 2. Comparisons of the AMS-measured mass concentrations to data reported by collocated instruments: (a) total (= SO_4^{2-} + NO_3^- + NH_4^+ + Cl^- + organics) versus $PM_{2.5}$ mass and apparent particle volume (D_m = 3–698 nm); (b) organics versus 2-hour- and 24-hour-averaged $PM_{2.5}$ OC; (c) sulfate versus $PM_{2.5}$ sulfate; (d) ammonium versus 4-hour-averaged $PM_{2.5}$ ammonium. See Table 2 for correlation coefficients. Plotted on the top of this figure are the time series of air temperature and relative humidity.

operate the vacuum system pumps continuously due to aircraft restrictions [*Bahreini et al.*, 2003].

3. Results and Discussions

3.1. Intercomparisons With Collocated Instruments

[23] Figure 2 shows the time series of the concentrations of particle mass (approximately NR-PM_1), organics, sulfate, and ammonium reported by the AMS, together with comparable traces from collocated instruments, including $PM_{2.5}$ mass measured by a tapered element oscillating microbalance (TEOM, Rupprecht & Patashnick Co., Inc, model 1400A, Albany, New York) that sampled at 30°C and was equipped with a Nafion diffusion dryer sample equilibration system (SES), along with a $PM_{2.5}$ inlet, apparent particle volume (calculated assuming spherical particles) measured by a scanning mobility particle sizer system (models 3936N25 and 3936L10, TSI, Inc.), 2-hour $PM_{2.5}$ OC measured in situ using a Sunset Laboratories thermal optical transmittance carbon analyzer [*Turpin et al.*, 1990] and 24-hour OC from manual undenuded filter samples (sampling details given by *Subramanian et al.* [2004]),

$PM_{2.5}$ sulfate measured with a semicontinuous sulfate analyzer (Rupprecht and Patashnick, model 8400S) similar to the nitrate instrument described by *Stolzenburg and Hering* [2003] and *Wittig et al.* [2004], and semicontinuous $PM_{2.5}$ NH_4^+ measured using a steam sampler [*Khlystov et al.*, 1995]. Note that $PM_{2.5}$ is defined on the basis of aerodynamic diameter measured at atmospheric pressure, which to first approximation equals the ratio of D_{va} to the square root of particle density for spherical particles. Overall the agreement of these comparisons is fairly good given the differences in size cutoff (Figure 2) and the correlation coefficients (r^2) are in the range of 0.64–0.88 (Figure 3).

[24] On the basis of the linear regression slopes, on average, the AMS reports ~66% of the total $PM_{2.5}$ mass observed by the TEOM and ~75% of the $PM_{2.5}$ sulfate from the semicontinuous SO_4^{2-} analyzer (Figure 3). These differences likely reflect the fact that the AMS measures PM_1 rather than $PM_{2.5}$ and that it has no response to refractory species, such as crustal, soot and metal components. *Drewnick et al.* [2004b] observed a similar regression slope (0.64) between the AMS and $PM_{2.5}$ TEOM data at Queens, New York, during the summer of 2001.

[25] Compared to those reported during two other field studies, the correlation coefficients (r^2) of particle mass and sulfate data measured by the AMS compared to those by TEOM and sulfate analyzer observed during this study (0.71 and 0.68, respectively) lie somewhat in the middle. During the PMTACS-NY summer 2001 campaign in Queens/New York, *Drewnick et al.* [2004a] reported very high r^2 (~0.9) between AMS-SO_4^{2-} and three semicontinuous $PM_{2.5}$ sulfate instruments, including particle into liquid sampler (PILS), R&P sulfate monitor (R&P 8400S), and a custom built continuous sulfate monitor. *Allan et al.* [2004a], however, observed a lower r^2 (~0.56) between SO_4^2 data from the AMS and those from the PILS during the ITCT 2K2 study at Trinidad Head, California. Similarly, the correlation between AMS-measured PM_1 mass concentrations and TEOM $PM_{2.5}$ mass was also significantly better during the PMTACS-NY study (r^2 = 0.91) [*Drewnick et al.*, 2004b] than during this study (r^2 = 0.71). It is not yet clear the exact reason for these differences, but more variable amounts of material between PM_1 and $PM_{2.5}$ in Pittsburgh as compared to New York might have played a role.

[26] Good correlation is observed between the AMS organic mass concentrations and 2-hour-averaged organic carbon concentrations measured by the Sunset Labs in situ carbon analyzer (r^2 = 0.88; Figure 3). This observation implies that the nominal particulate organic mass to carbon ratios (i.e., OM:OC ratios) are mostly in the range 1.2 to 2.2, with a regression slope of ~1.7 (larger if differences in size cutoff, i.e., PM_1 versus $PM_{2.5}$, are accounted for). This value is similar to the OM:OC ratio (1.6 ± 0.2) recently estimated for urban organic aerosols [*Turpin and Lim*, 2001]. Although the actual values are expected to change with time because of their dependence on organic aerosol types (the values are likely smaller in the morning when significant amounts of fresh combustion organic aerosols (OM:OC ratio ~ 1.2) are emitted and larger (e.g., OM:OC ratio ~ 2.0) in the afternoon when organics are more oxidized and secondary in nature [*Russell*, 2003; *Turpin and Lim*, 2001]), we did not observe significant diurnal variations in OM:OC ratios. One possible explanation for this is that ambient PM_1 organics in Pittsburgh is often dominated by regional aged particles [*Anderson et al.*, 2004; *Tang et al.*, 2004], and thus show less pronounced difference in OM:OC ratios between morning and afternoon. *Cabada et al.* [2002], for instance, estimated that up to 50% of the organic aerosol mass in Pittsburgh is of secondary origin during the summer. Our AMS mass spectra also suggest that there was a relatively high concentration of oxygenated organic aerosols during most periods in this study (Zhang et al., submitted manuscript, 2004).

[27] Present analytical uncertainties of the AMS might have also contributed to the lack of significant differences in the ratios of the AMS organic mass to the organic carbon content, between periods that appeared to be dominated by different types of organic aerosols. The AMS organic data may suffer from compensating systematic biases due to the application of constant relative ionization efficiency (RIE) and collection efficiency (CE; see section 2.3.2) for organic signals. According to *Jimenez et al.* [2003c] the expected RIE of oxygenated organics is somewhat lower than that of the hydrocarbons. However, we have used the average of these two types of organic aerosols (i.e., RIE = 1.4; Table 1), which probably has led to an overestimation of the mass concentrations of primary organic aerosols and an underestimation of those of the secondary. Similarly, using a constant CE, which can be different for different organic aerosol types, might have introduced analytical errors as well. A procedure of separating the contributions of primary and oxidized organics aerosols (using both the size distributions and the mass spectra from the AMS) is currently under development and will be presented in a future publication (Zhang et al., submitted manuscript, 2004). This technique will permit the application of different RIE and CE factors to primary and oxidized aerosols, which may increase the variability of the OM:OC ratios.

[28] Given that the AMS and the SMPS during this study appear to measure a relatively similar particle population (detailed in paragraphs below and in Figure 4), the regression slope of the AMS mass concentrations and the SMPS volume concentration provides an estimation for the density of bulk particles in Pittsburgh, i.e., ~1.4 g cm^{-3}. However, as shown in Figure 3, the correlations between these two measurements appear to separate into two groups. The likely reasons for the separation are the effects of particle shape (see Figure 4a and associated discussions) and density. Further work in our group is in progress to address this apparent discrepancy by quantitative simultaneous modeling of the AMS and SMPS data [*DeCarlo et al.*, 2004; *Slowik et al.*, 2004].

[29] We estimated that the typical dry density of the nonrefractory PM_1 in Pittsburgh is roughly 1.55 g cm^{-3} on the basis of the average particle composition of ~65% inorganics (i.e., SO_4^{2-}, NH_4^+, and NO_3^-) and ~30% organics (see section 3.2), plus 5% of black carbon, and the assumption that the densities of $(NH_4)_2SO_4$, NH_4NO_3, bulk organics, and black carbon are ~1.78, 1.72, ~1.2 g cm^{-3} [*Turpin and Lim*, 2001], and 1.77 g cm^{-3} [*Park et al.*, 2004] respectively. Black carbon was estimated from AMS *m*/*z* 57 during the periods in which it was not available since these measurements were strongly correlated (r^2 = 0.78; slope = 0.11 μg m^{-3}/μgC m^{-3}) (Zhang et al., submitted manuscript, 2004). Note that the estimated densities

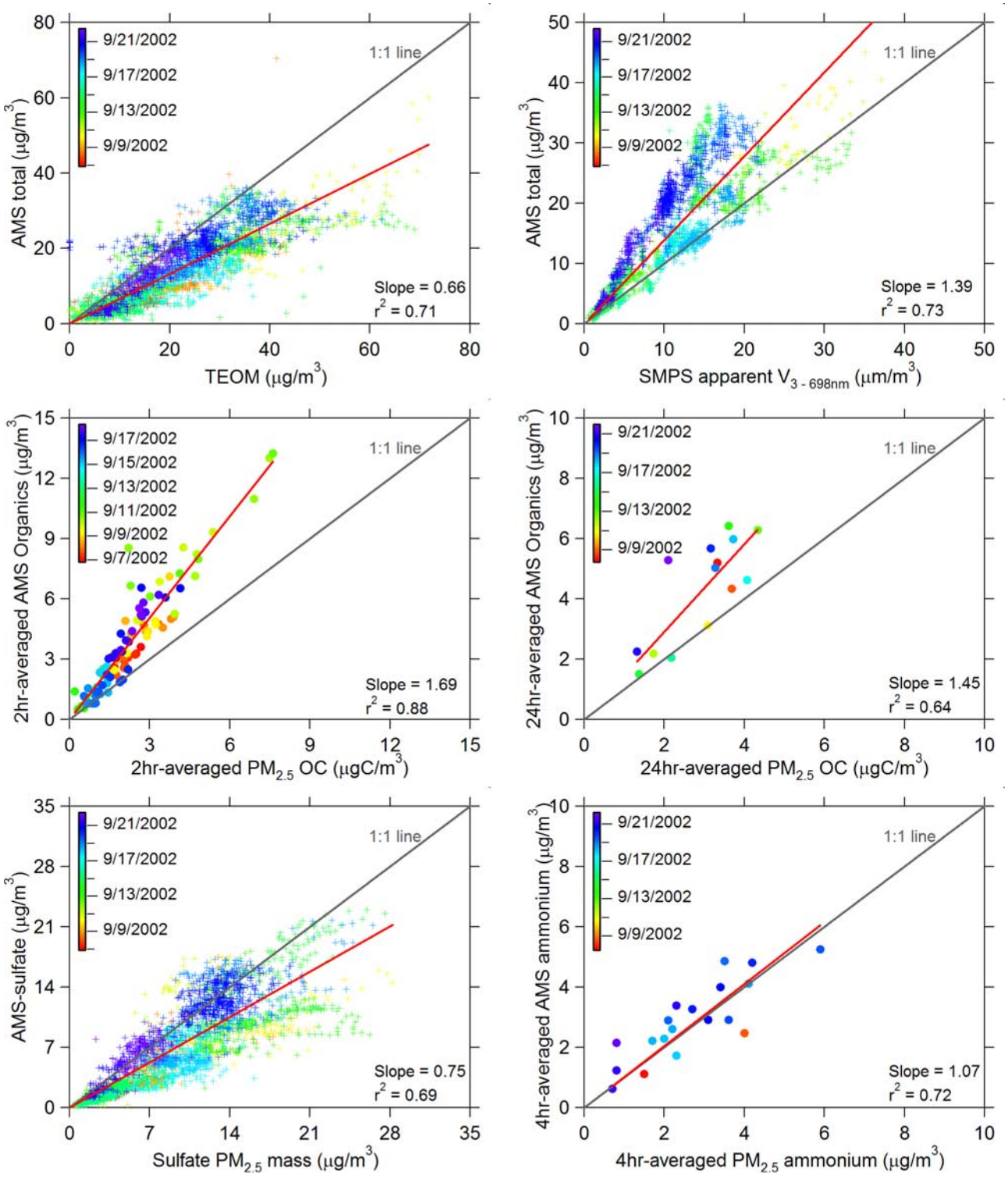

Figure 3. Correlation plots of AMS-measured mass concentrations versus data reported by collocated instruments. Data points are colored by time. Red lines are linear fits to the data.

reported in this study may contain systematic errors because refractory species other than black carbon, such as metals and crustal components, are not detectable by the AMS. However, refractory species other than black carbon on average only contribute <10% of the total mass of PM_1 in Pittsburgh [*Cabada et al.*, 2004]. Thus the error in the estimated density due to the omission of metals and crustal components is expected to be small. *Wittig et al.* [2004] reported a similar value, 1.5 g cm^{-3}, for the bulk density of the ambient particles in Pittsburgh, on the basis of TEOM and SMPS measurements.

[30] Figure 4 compares the AMS to the SMPS on the average size distributions of particle mass during 3 representative periods. The AMS data are the sum of SO_4^{2-}, NH_4^+,

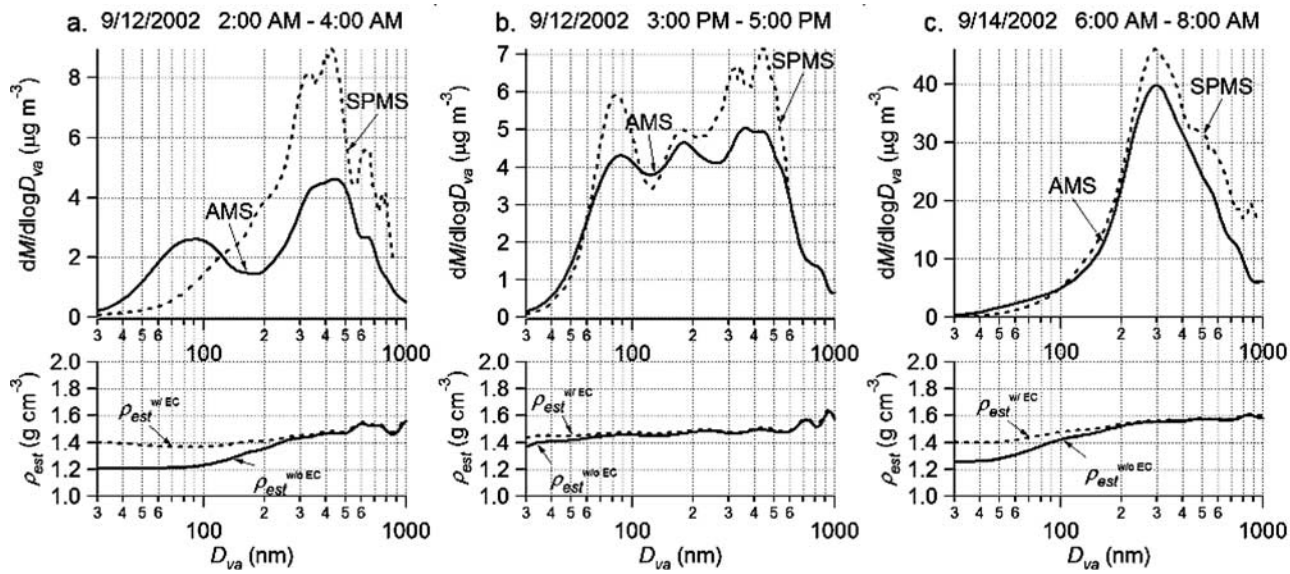

Figure 4. (a–c) Comparisons of 2-hour-averaged particle mass distributions measured by the AMS to those calculated from the SMPS number distribution data assuming spherical particles and $D_{va}/D_m = \rho_{est}^{w/EC}$. $\rho_{est}^{w/EC}$ (dashed lines) is the size-resolved particle density estimated on the basis of the mass distributions of particle species and assuming an average density of 1.77 g cm^{-3} for inorganics (SO_4^{2-} + NH_4^+ + NO_3^-), 1.2 g cm^{-3} for organics, and 1.77 g cm^{-3} for black carbon. Since the black carbon size distribution was estimated (see text), $\rho_{est}^{w/oEC}$ (solid lines), which is the particle density estimated only using the AMS inorganic and organic data (i.e., not including the contributions of black carbon), is shown as a comparison.

NO_3^-, and organics. The distributions of SMPS mass concentrations (M) were calculated from the number distribution data [*Jimenez et al.*, 2003a, 2003b]:

$$M = \pi/6 \times D_m^3 \times \rho_{est} \quad (1)$$

$$D_{va} \approx D_m \times \rho_{est} \quad (2)$$

where D_m is the mobility diameter reported by the SMPS and ρ_{est} is the estimated density of nonrefractory particles weighted by AMS-measured particle composition assuming an average density of 1.77 g cm^{-3} for inorganic species and ~1.2 g cm^{-3} for organics [*Turpin and Lim*, 2001].

[31] In order to examine the influence of black carbon on estimated particle density, we have estimated the size distributions of elemental carbon (EC) during this study. Our approach is based on the findings that an AMS mass spectral signature, m/z 57, is a good tracer for primary combustion related organic aerosols [*Alfarra et al.*, 2004; Zhang et al., submitted manuscript, 2004]. Good correlation has been observed between the mass concentrations of m/z 57 and those of EC (r^2 = 0.78; slope = 0.11 μg m^{-3}/μgC m^{-3}) during this study (Zhang et al., submitted manuscript, 2004). While some dependence of the density, and thus OC/EC ratio, of diesel soot particles versus mobility diameter has been shown [*Park et al.*, 2004], this dependence is significantly reduced when considered versus D_{va} [*Slowik et al.*, 2004]. Thus we estimated the size distribution of elemental carbon (in D_{va} space) to be the same as that of m/z 57. We subsequently calculated the estimated density of particles including the EC contribution assuming an EC density of 1.77 g cm^{-3} [*Park et al.*, 2004] and along with information about the inorganic and organic components. The effect of EC in the estimated density is very small for the accumulation mode, but is more important for smaller particles and for periods where combustion emission concentrations are larger (e.g., Figure 4a).

[32] The average mass distributions obtained by the AMS and the SMPS agree quite well for 2 periods (Figures 4b and 4c), but at 2:00–4:00 am, 12 September, the AMS reported significantly larger mass of small particles (D_{va} < ~120 nm) and significantly lower mass of accumulation mode particles (D_{va} ~ 200–700 nm) than the SMPS did (Figure 4a). Such discrepancy has been frequently observed in urban areas when comparing the AMS and SMPS data, and is attributed to the presence of a significant amount of small irregularly shaped particles (e.g., soot from traffic emissions). This is because the AMS and the SMPS respond differently to particle shape: as a particle becomes less spherical, the AMS-measured D_{va} decreases while the SMPS-measured D_m increases [*Jimenez et al.*, 2003a, 2003b; *DeCarlo et al.*, 2004]. This effect also leads to an overestimation of the accumulation mode by the SMPS, due to irregular particles that appear larger than they really are (and thus have much more apparent than real volume). Indeed, we found that the ultrafine particles during 2–4 am on 12 September were almost pure organic (average estimated density including EC contributions, i.e., $\rho_{est}^{w/EC}$, ~1.4 g cm^{-3}) while those from the other two periods contained significantly more inorganics (resulting in higher $\rho_{est}^{w/oEC}$; Figure 4a).

[33] In general, these two instruments agree well on the size distributions of the accumulation mode particles for periods b and c, although the AMS reports slightly lower

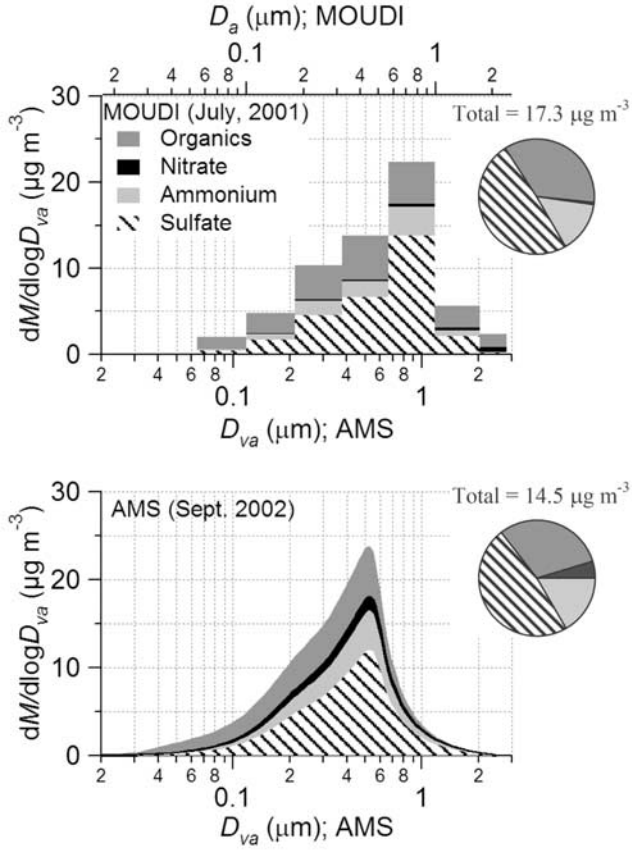

Figure 5. Comparisons of size-resolved chemical compositions measured by the AMS during September 2002 to those of a MOUDI during July 2001. Note that "D_a" is the aerodynamic diameter measured by MOUDI. Given that diameter measurement in MOUDI is operated under higher pressure than that within the AMS to first approximation $D_{va}/D_a \approx \rho_{est}^{1/2}$.

mass concentrations than the SMPS does at these sizes. Besides the possible influence from particle shape, another reason for such discrepancy is that the AMS does not measure refractory components, such as the mineral and crustal materials. It is interesting to note the comparatively good agreement between the SMPS and AMS on the distributions of the ultrafine particles during 3–5 pm, 12 September (Figure 4b). The reason is that a major fraction of these particles were the product of extensive condensational growth of the new particles that formed in a regional intense nucleation event that happened in the morning of 12 September [*Zhang et al.*, 2004]. These particles appeared to be relatively spherical and as such the AMS and the SMPS detect them similarly.

[34] We also compared the average size-resolved chemical composition data determined by the AMS in this study (September 2002) to those obtained with a micro-orifice uniform deposit impactor (MOUDI) for July 2001 (Figure 5). The results from the two instruments are similar at D_{va} below ~0.8 μm, despite the different sampling time periods. This is not surprising since the general characteristics of the particles during these two long averaging periods are expected to be similar given the major regional contributions to fine particle concentrations in Pittsburgh, the likely similar local emission mix, and the similar season of sampling (July versus September) [*Anderson et al.*, 2004; *Tang et al.*, 2004; *Wittig et al.*, 2004]. In addition, in order to better compare the AMS and MOUDI mass distributions, we plotted the MOUDI data onto D_{va} space using the following simplified equation [*Canagaratna et al.*, 2004; *Jimenez et al.*, 2003a, 2003b]:

$$D_{va} \approx D_a \times \rho_{est}^{1/2} \quad (3)$$

where D_a is the aerodynamic diameter measured by MOUDI and ρ_{est} is the estimated density of particles (Figure 5). In this way, the average mass distribution of Pittsburgh particles in July 2001 appears to peak at D_{va} of ~0.8–1 μm. The differences between the AMS and MOUDI at D_{va} > 600 nm might be due to less than unit transmission of the AMS for particles larger than 600 nm (i.e., the approximately PM_1 cut of the AMS versus the $PM_{2.5}$ cut of the MOUDI). This comparison is consistent with the differences between the concentrations of particle mass and sulfate measured by the AMS and TEOM and the sulfate analyzer (Figures 2 and 3) are partly due to the difference size cuts of the instruments (i.e., PM_1 versus $PM_{2.5}$), although it is not a proof due to the different sampling periods. Similar findings have been reported by *Alfarra et al.* [2004].

[35] Note that a mass closure test, i.e., a thorough evaluation of the differences between the mass concentrations measured by the AMS and those of the TEOM would be very valuable. However, it is not possible to perform such a test for this data set since MOUDI data, as well as data for some refractory components such as minerals and metals, are not available for this period.

3.2. Particle Characteristics and Dynamics

3.2.1. Mass Concentrations

[36] The temporal variations of the mass concentrations of NR-PM_1 SO_4^{2-}, NH_4^+, NO_3^-, organics, Cl^-, and total (= SO_4^{2-} + NH_4^+ + NO_3^- + organics + Cl^-) are shown in Figure 6. Sulfate (for ~70% of the time during this study), and less frequently organics (for ~30%), dominates the particle composition. The mass concentrations of ammonium are relatively high as well, and are well correlated with those of sulfate (r^2 = 0.83; Figure S1 in the auxiliary material[1]). These two species together account for more than half of the total NR-PM_1 mass for over 75% of the sampling time of this study.

[37] The correlation between the mass concentrations of organics and sulfate is relatively weak (r^2 = 0.41; Figure S1 in the auxiliary material). Our interpretation for this observation is that local traffic emissions contribute significantly to the organic particle concentrations while the ambient concentrations of particulate sulfate are likely mainly driven by regional accumulation rather than local emissions. However, these two species appear to be internally mixed in the accumulation mode, as suggested by the good correlation between the mass concentrations of organics and sulfate in

[1]Auxiliary material is available at ftp://ftp.agu.org/apend/jd/2004JD004649.

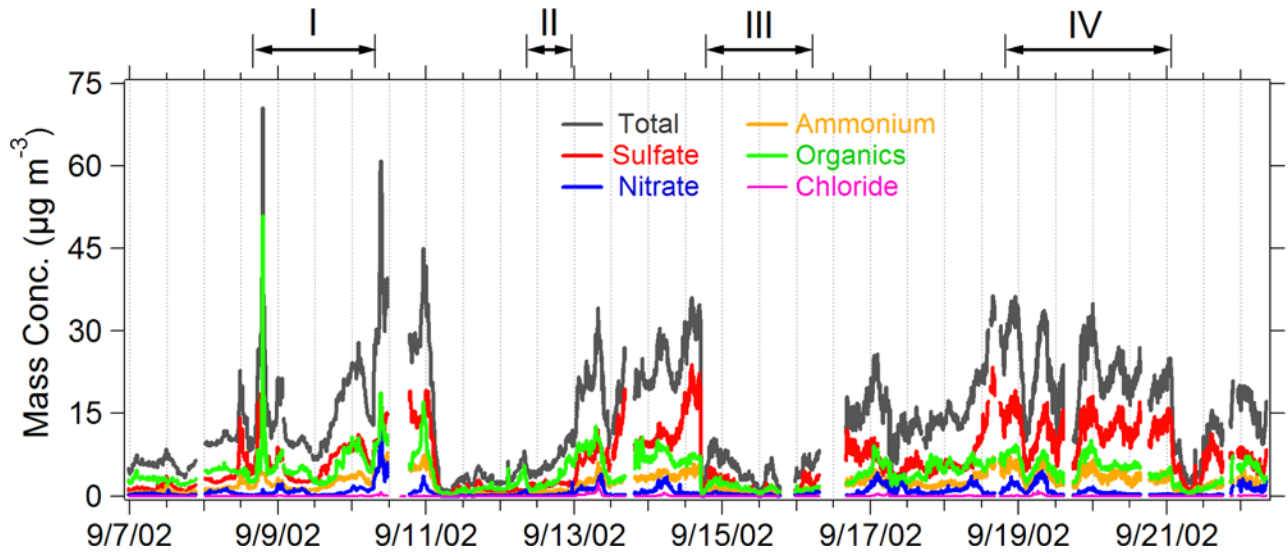

Figure 6. Times series of the mass concentrations of SO_4^{2-}, NO_3^-, NH_4^+, Cl^-, organics, and total (= SO_4^{2-} + NO_3^- + NH_4^+ + Cl^- + organics). Periods I, II, III, and IV are marked as references for Figure 7.

the 250–1000 nm size range (see section 3.3.2.). Indeed, internally mixed organics and sulfate in Pittsburgh fine particles have been observed by *Bein et al.* [2005] using a rapid single-particle mass spectrometer (RSMS). In addition, similar findings have been reported in studies at other locations using single-particle MS techniques, such as particle analysis by laser mass spectrometry (PALMS) [*Lee et al.*, 2003, and references therein].

[38] Nitrate and chloride are generally low and both show very weak correlations with sulfate ($r^2 < 0.1$). The mass concentrations of NO_3^- are likely controlled by partitioning or formation of nitric acid. Since NaCl is not measured by the AMS at the vaporizer temperature used in this study the detected chloride must originate either from more volatile inorganic chlorides (such as NH_4Cl) or from organic chlorine-containing species. We observed some correlation ($r^2 \sim 0.30$, Figure S1 in the auxiliary material) between NO_3^- and Cl^-, probably due to the fact that the formation of NH_4NO_3 and NH_4Cl is favored by the same conditions: higher NH_3 in the gas-phase and higher RH.

[39] Multiday episodes of fine particle pollution, with intermittent cleaner periods, are observed (Figure 6). The cleaner periods often start with heavy rainfall (e.g., ~5 pm on 14 September and ~6 am on 21 September) and/or the arrival of clean air from Canada (e.g., ~1–4 am on 11 September), which quickly reduce the mass concentrations of NR-PM_1 by one to two orders of magnitude. Afterward, the particle mass loading gradually increases but remains low for 1–3 days. Most significant and lasting increases of aerosol mass concentrations are associated with rapid increases of sulfate. Several short-lived spikes of organic aerosols are detected, likely due to the passage of relatively fresh local plumes by the sampling site. The mass spectra and size distributions of these organic aerosols suggest that they originated from combustion sources.

3.2.2. Size Distributions

[40] Figure 7 shows the average size distributions and chemical compositions of NR-PM_1 during 4 periods (marked as I, II, III, and IV on Figure 6) of this study. These periods were selected to represent various aerosol "climatologies" observed in this study: Period I is relatively polluted with approximately equal amounts of sulfate and organic aerosols; II corresponds to the growth stage of a strong regional nucleation event [see *Zhang et al.*, 2004]; III is a relatively clean period after a rain shower; and IV is a sulfate-dominated regional pollution episode.

[41] The mass distributions are significantly different during these 4 periods, showing unimodal, bimodal and even trimodal characteristics. An accumulation mode peaking between 350–600 nm (D_{va}) is constantly observed. This mode appears to be an internal mixture of ammonium sulfate with variable amounts of organics and a minor fraction of nitrate. In general, as the aerosol mass concentration increases and for more aged particles (e.g., in period IV), the peak diameter of the accumulation mode increases, the distribution appears to be narrower (e.g., the geometric standard deviations σ_g of total mass distributions were ~2.0 and 1.6 for periods III and IV, respectively), and the sulfate content increases (Figure 7). However, the size distributions reported here are "as measured" and could be skewed by the limited aerodynamic lens transmissions for particles larger than 600 nm and smaller than 60 nm in D_{va} [*Jayne et al.*, 2000]. Details in evolution of the mass distributions of particle species during this entire study are presented in Figures S4 and S5 in the auxiliary material.

[42] In addition to the accumulation mode, two smaller modes, one below 100 nm and one at ~200 nm, are also frequently observed (e.g., Figure 7, periods I and II). Given the essentially same size distributions of NH_4^+ and SO_4^{2-} throughout the entire campaign, and the good correlations between their mass concentrations (see section 3.2.1), these two species appear to be internally mixed, likely in the forms of $(NH_4)_2SO_4$ and NH_4HSO_4, in all modes. The organics, however, very often show an ultrafine mode ($D_{va} < 100$ nm) that seems to be externally mixed with the other species. We have evidence that fuel combustion,

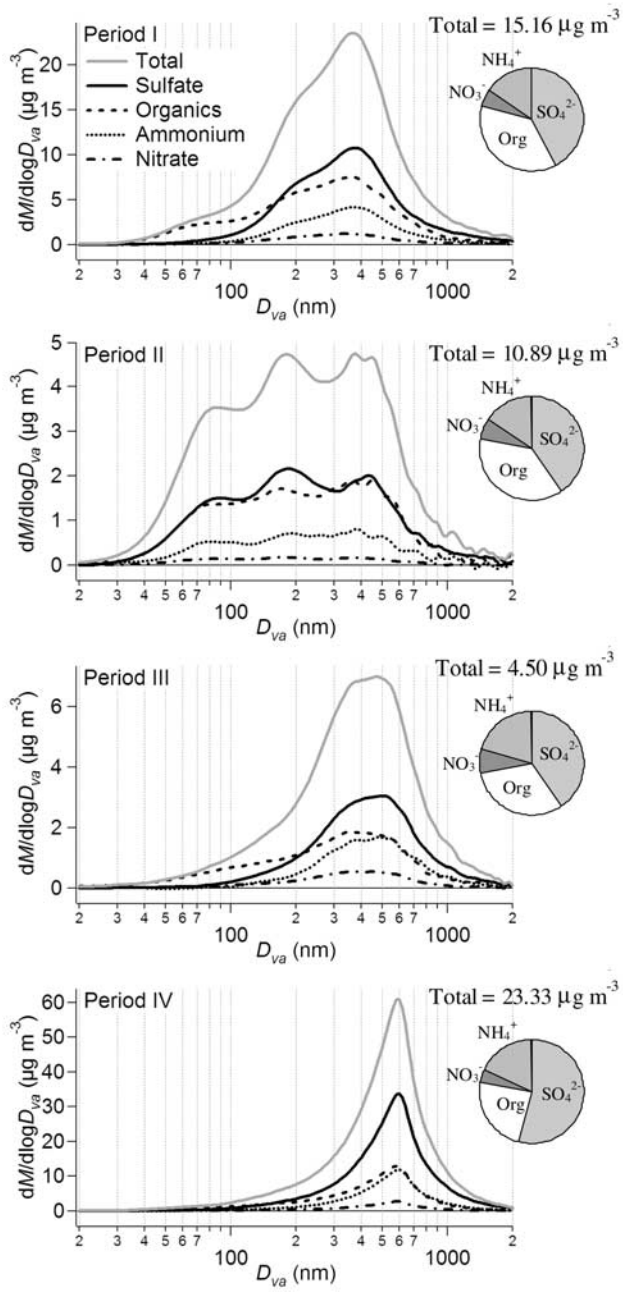

Figure 7. Average size distributions and chemical compositions of particle species during four time periods with similar characteristics (i.e., periods I, II, III, and IV as marked in Figure 6) of this study.

i.e., traffic emissions (see section 3.3.2) is a major source of these small mode organic aerosols. Similar findings have been reported for AMS measurements in other urban areas [e.g., *Alfarra et al.*, 2004; *Boudries et al.*, 2004; *Drewnick et al.*, 2004c]. *Canagaratna et al.* [2004] also reported a peak D_{va} of ~90 nm on the mass-weighted size distributions of the fresh diesel exhaust particles.

[43] Ultrafine particles behave rather differently during period II, the particle growth stage of a strong regional nucleation event that started at ~8:00 am. These particles consist of comparable amounts of sulfate and organics, which appear to be an internal mixture, together with NH_4^+ and NO_3^- (Figure 7, period II). In fact, given the similarities in their size distributions, SO_4^{2-}, NH_4^+, NO_3^-, and organics appear to be internally mixed over the entire size range during period II. Such homogeneity in aerosol composition was developed through extensive condensation of gas phase species including H_2SO_4, NH_3, HNO_3, and photochemically processed organic species, a phenomenon that is commonly observed during the growth stage of nucleation events in Pittsburgh. The reader is referred to *Zhang et al.* [2004] for a detailed description on the evolution of particle compositions and size distributions during this nucleation event.

[44] The average size distribution of particle mass concentration of the entire sampling period demonstrates a broad peak at ~550 nm (D_{va}), a slight shoulder at around 200 nm, and a tail that extends below 100 nm (Figure 8a). The composition of the particles changes as a function of size in that larger particles tend to contain more SO_4^{2-} and NH_4^+ and less organics (Figure 8b). As a result, the estimated particle density is strongly size dependent as well, with higher values for the larger particles (Figure 8c). Note that mineral species have not been taken into account since they are not detectable by the AMS and their size-resolved measurements were not available during this study. As described above, this omission should only cause a small error in the estimated density.

[45] Sulfate is the major component of the accumulation mode while organics dominate the mass of particles smaller than 200 nm (D_{va}). Despite the high frequency of nucleation events in Pittsburgh [*Stanier et al.*, 2004] and the fact that the ultrafine particles produced during the nucleation events are mainly composed of SO_4^{2-} and NH_4^+ [*Zhang et al.*, 2004], organics overall account for up to 80–90% of the ultrafine mass (D_{va} < 100 nm) (Figure 8b). This observation is consistent with combustion emissions being the major source of ultrafine mass in Pittsburgh, since the nonrefractory fraction of ultrafine particles from combustion processes are usually almost completely organic [*Canagaratna et al.*, 2004]. A detailed analysis on the possible sources of organic species in Pittsburgh will be presented in a future publication (Zhang et al., submitted manuscript, 2004).

[46] In addition to the accumulation mode and the ultrafine mode particles, there also appears to be an intermediate mode ($D_{va} \approx 100-250$ nm) that is composed of comparable amounts of SO_4^{2-} and organics. The size ranges of these particles correspond to the so-called condensation mode [*Pandis et al.*, 1995] and are likely the condensational growth products of the ultrafine particles from primary emissions or formed during the nucleation events. Conceptually these particles may be "on their way" to the accumulation mode, but not yet had enough time, or had not been through cloud or fog processes [*Pandis et al.*, 1995], to grow to that size yet. These AMS-measured mass distributions are consistent with measurements by MOUDI at the same site during the summer of 2001 [*Cabada et al.*, 2004].

3.2.3. Diurnal Variations of Mass Concentrations and Size Distributions

[47] A summary of the diurnal cycles of SO_4^{2-}, NH_4^+, NO_3^-, and organics is shown in Figure 9. Note that the dips at the eighteenth hour on the plots are biased by a very large

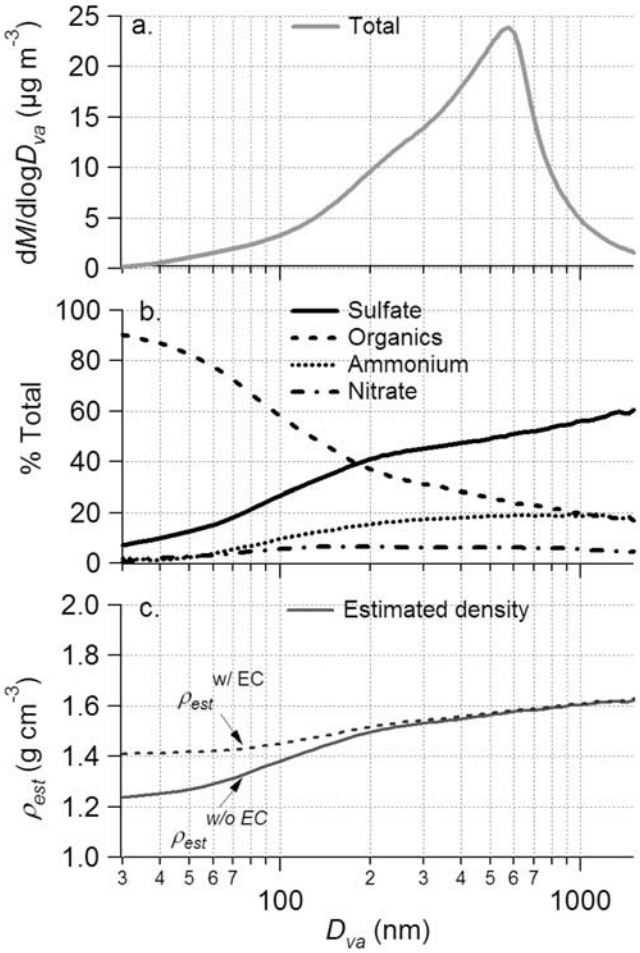

Figure 8. Averaged size distributions of (a) total nonrefractory mass, (b) particle chemical composition, and (c) estimated density for nonrefractory particle components (solid line) and estimated particle density including the contribution of elemental carbon (EC) (dashed line) averaged over the entire study (7–22 September 2002).

and sharp drop in particle concentration between 17:00 and 18:00 on 15 September, due to heavy rainfall (see Figure 6). The mass concentration of sulfate does not show a pronounced diurnal cycle, but nonetheless demonstrates a slight increase during the day (Figure 9a). Such increase appears to be driven by enhanced photochemical production of gaseous H_2SO_4. However, the overall lack of a clear diurnal cycle of sulfate suggests that multiday accumulation of sulfate on a regional scale dominates over its same-day photochemical production. The average concentrations of ammonium also slightly increased during the afternoon (Figure 9b), probably a result of neutralization of the enhanced H_2SO_4 uptake.

[48] The mass concentration of nitrate shows a pronounced diurnal profile that peaks in the early morning, drops after 10 am, and stays at low levels between 12:00 noon and 7:00 pm (Figure 9c). The observed cycle is likely partially driven by the gas-to-particle partitioning of ammonium nitrate precursors (gaseous HNO_3 and NH_3), which is favored by the lower temperature and higher relative humidity during the night and the early morning [*Seinfeld and Pandis*, 1998]. In addition, the higher level of nighttime gaseous N_2O_5 and NO_3, which are quickly photolyzed during the day, might have acted as a significant source of NO_3^- concentrations at night [*Brown et al.*, 2003a, 2003b; *Pandis et al.*, 1995] while enhanced higher particle acidity in the afternoon, as suggested by a relatively steeper increase of SO_4^{2-} than NH_4^+ between 1:00 pm and 4:00 pm (Figures 9a and 9b), might have played a role in reducing the concentration of NO_3^- in the particles during that period.

[49] The average mass concentrations of organics are somewhat higher at night (Figure 9d), which might be attributed to the lower mixing layer depth that traps the city emissions. In addition, a small peak of organic mass is observed during the morning rush hour between 7:00–9:00, reflecting the fact that traffic emissions are usually an important source of organic aerosols in urban areas. *Drewnick et al.* [2004b] reported similar diurnal behaviors of SO_4^{2-}, NO_3^-, and organics at Queens, New York, during July 2001.

[50] Figures 9e–9h are the average size distributions of the species during two time periods of the day, 6–9 am EST (i.e., 7–10 am EDT; the morning rush hours) and 1–4 pm (i.e., the period of most intense photochemistry and accumulation of photochemically produced aerosols). The average size distributions of SO_4^{2-}, NH_4^+, and NO_3^- are similar to each other in the morning (6–9 am) as well as in the afternoon (1–4 pm). A much broader distribution of the organics, however, is observed during the morning rush hour, indicating the presence of large amounts of traffic-related small mode organic aerosols.

[51] The average size distribution of organics is much narrower during 1–4 pm and becomes very much alike to those of the inorganic species (Figure 9h). It appears that the organic aerosols from morning traffic emissions have been diluted by the increase of the mixing layer height and evolved by coagulation and/or condensation of gas phase species.

3.2.4. Particle Acidity

[52] We evaluated the acidity of the particles by comparing measured NH_4^+ mass concentration to the amount needed to fully neutralize the measured SO_4^{2-}, NO_3^- and Cl^-. Particles are considered "more acidic" if the measured NH_4^+ concentration is significantly (by 25% or more) lower than the predicted values, and as bulk neutralized if the two values are similar. A measured-to-predicted NH_4^+ ratio of 0.75 suggests that roughly 50% of the SO_4^{2-} molecules in the particles are in the form of bisulfate (HSO_4^-). This approach should be relatively accurate because Pittsburgh particles generally contain very low amounts of the metal ions, such as Na^+, Ca^{2+} and K^+ [*Rees et al.*, 2004; *Wittig et al.*, 2004].

[53] On the basis of this definition, aerosols appear to be bulk neutralized to slightly acidic for the majority of the time, but there are also episodes when they are "more acidic" (Figure 10). We estimate that for roughly 20% of the time during this study the measured-to-predicted NH_4^+ ratios are less than 0.75, i.e., the mole ratio of NH_4HSO_4 to $(NH_4)_2SO_4$ is above 1 (Figure 10b). Because the acidic particles are often found during the high-mass-loading periods and only show a weak correlation with UV × SO_2, which is a proxy for gas-phase H_2SO_4 production

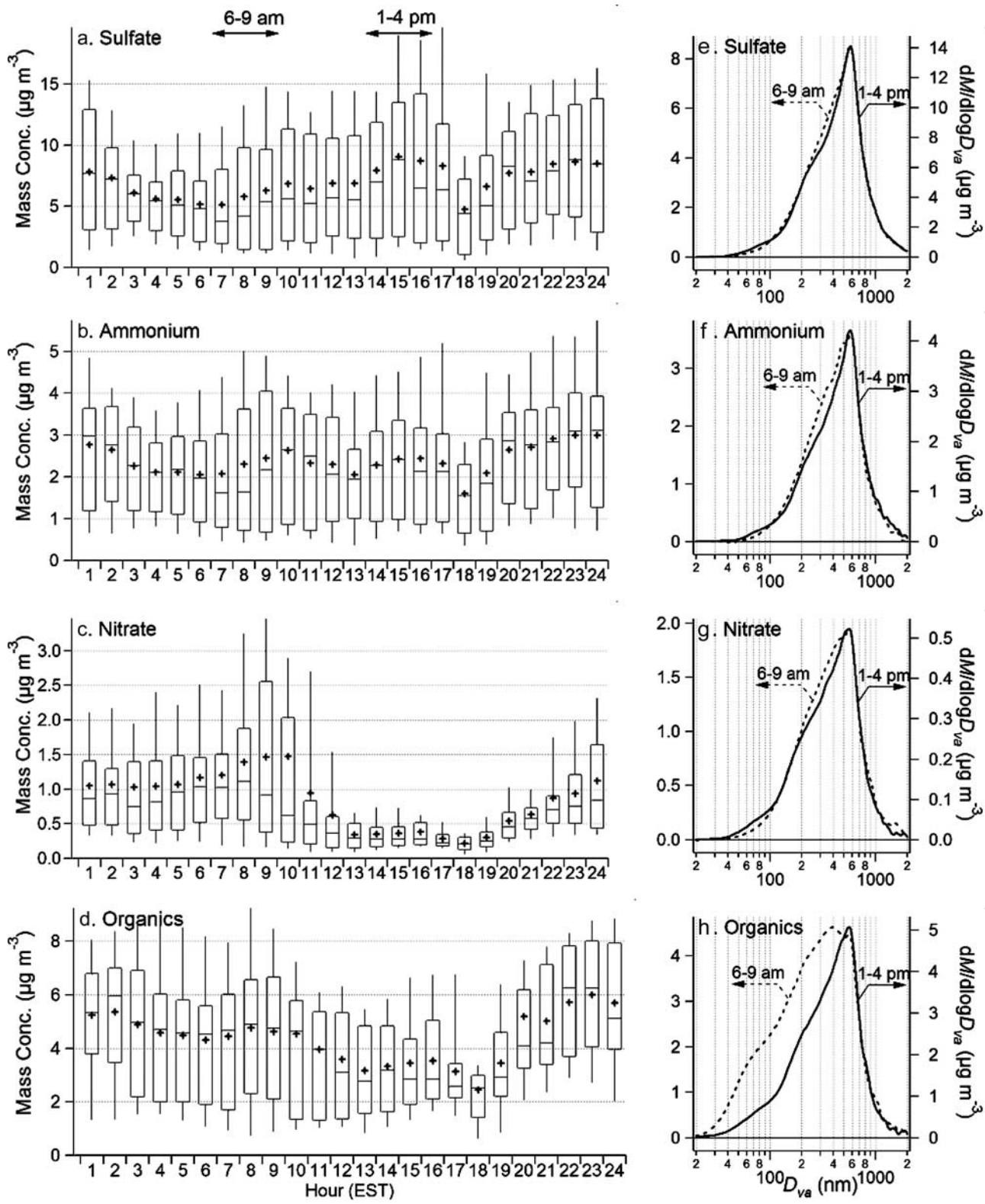

Figure 9. Average diurnal cycles of the mass concentrations of (a) SO_4^{2-}, (b) NH_4^+, (c) NO_3^- and (d) organics and (e–h) the average size distributions of particle species during 6–9 am and 1–4 pm (7–22 September 2002). The box plots are read as follows: the upper and lower boundaries of the box indicate the 75th and the 25th percentiles, the line within the box marks the median, and the whiskers above and below the box indicate the 90th and 10th percentiles. Cross symbols represent the means. The x-axis labels of the diurnal plots correspond to the hour of the day, e.g., "1" means from 00:00–01:00 am.

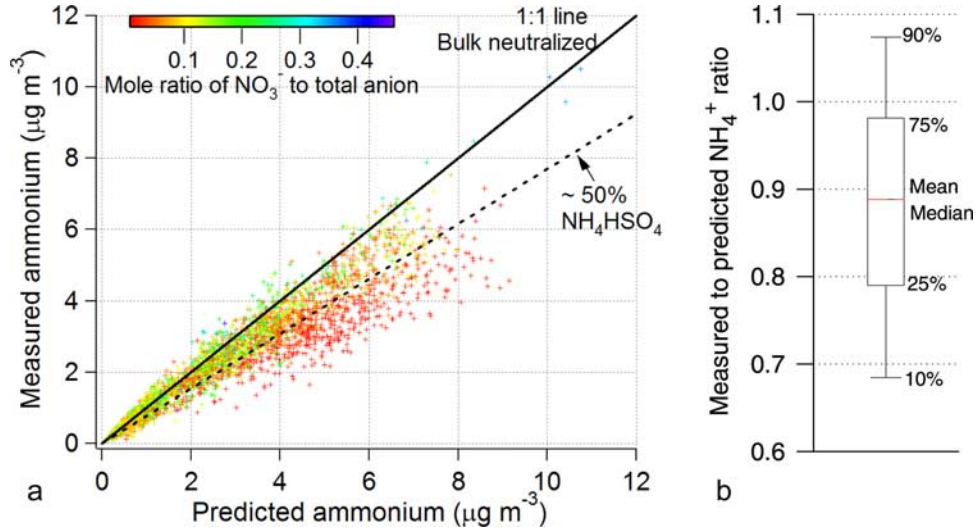

Figure 10. (a) Mass concentrations of measured NH_4^+ versus predicted NH_4^+ and (b) box plot of the ratio of measured to predicted NH_4^+ during the entire study (7–22 September 2002 EST). Note that predicted NH_4^+ concentrations were calculated from measured SO_4^{2-}, NO_3^-, and Cl^- assuming full neutralization of these anions by NH_4^+.

rate, we speculate that they are particles transported from large plumes relatively depleted of NH_3.

[54] Summarized in Figure 11 are the average compositions of neutralized (i.e., measured-to-predicted NH_4^+ ratio ≈ 1.0) and "more acidic" (i.e., measured-to-predicted NH_4^+ ratio < 0.75) particles. Compared to those considered as neutralized, the "more acidic" particles on average contain ~30% more mass, which is almost exclusively due to the increase of SO_4^{2-}. These two types of particles, however, contain comparable amounts of organics and NH_4^+. Within the limitations of this analysis, we observe negligible enhancement on the organic concentration that could be attributed to acid-catalyzed secondary organic aerosol formation [*Jang et al.*, 2002]. In addition, the concentrations of NO_3^- and Cl^- in the "more acidic" particles are roughly half of those in the neutralized particles, probably because of displacement of HCl and HNO_3 by H_2SO_4 in the competition for NH_3 [*West et al.*, 1999].

3.3. Primary and Secondary Aerosol Sources and Processes

3.3.1. Gas to Particle Partitioning of Nitrate

[55] In order to investigate the diurnal cycles of the particulate nitrate mass, we plotted in Figure 12 the average diurnal patterns of NO_3^- together with UV × NO_2, which is a proxy for daytime HNO_3 production rate, and the equilibrium formation constant of NH_4NO_3 from gas phase HNO_3 and NH_3 (i.e., K_p, ppb^{-2}). The K_p defined here is the inverse of the product of the partial pressures of NH_3 and HNO_3, and thus it is calculated using the inverse form of equation 9.91 of *Seinfeld and Pandis* [1998]:

$$\ln K_p = 1/(84.6 - 24220/T - 6.1\ln(T/298))$$

where T is the ambient temperature in Kelvin. Although this equation only applies to dry particles, the relative trend of partitioning versus temperature is exactly the same when particles contain liquid water (equation 9.92 of *Seinfeld and Pandis* [1998]).

[56] The diurnal profile of the CO concentrations is also included as a first-order indicator for daily changes in the boundary layer height. Overall, the diurnal patterns of NO_3^-, K_p and CO positively correlate, but all anticorrelate with that of UV × NO_2 (Figure 12). Although the morning peaks of NO_3^-, CO, and K_p are shifted by about 1–2 hours, these comparisons nonetheless suggest that variations in the

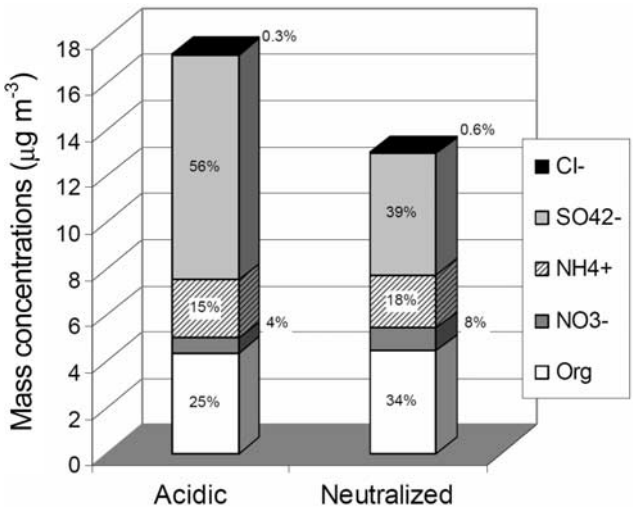

Figure 11. Average compositions of neutralized and "more acidic" NR-PM_1 particles during 7–22 September 2002. The neutralized particles are defined as those with measured-to-predicted ratio of NH_4^+ between 0.93 (the mean value) and 1.15 (90th percentile), and the "more acidic" particles are those with a ratio of less than 0.75, i.e., those that contain approximately equal moles of NH_4HSO_4 and $(NH_4)_2SO_4$.

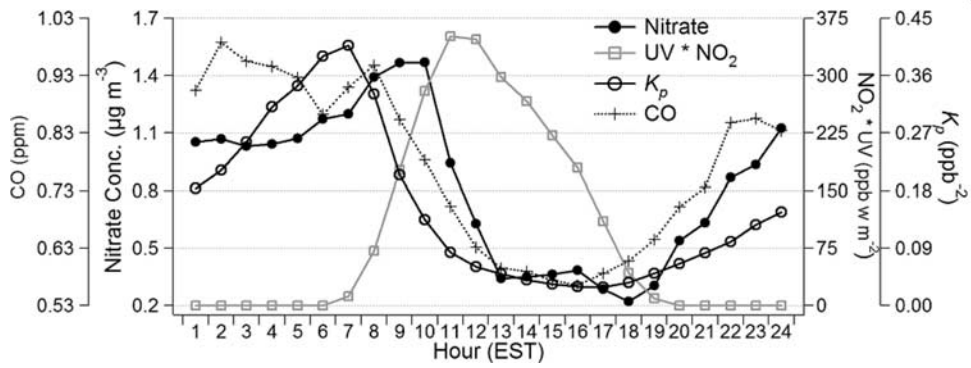

Figure 12. Average diurnal variations of 1-hour-averaged NO_3^- concentrations, CO, UV × NO_2, and the equilibrium constant for NH_4NO_3 formation (K_{sp}) during 7–22 September 2002.

mixing layer depth and gas to particle partitioning of HNO_3 appear to have played important roles in driving the diurnal cycles of the particulate NO_3^- concentrations. On the other hand, the fact that the NO_3^- concentrations remain high for ~2 hours after ~7:00 am, when in general K_p starts to decline and boundary layer height begins to increase, suggests that either photochemical production of HNO_3 or transport of nitrate particles are responsible for maintaining the NO_3^- level during this period of time. Despite the relatively higher photochemical production of HNO_3 in the afternoon, this mechanism does not result in increased NO_3^- concentrations during that time period.

3.3.2. Combustion Sources and Photochemical Formation of Organic Aerosols

[57] In addition to the average size distributions (see section 3.2.3), the average mass spectra of organic aerosols are also considerably different between the morning rush hours (i.e., 6–9 am EST or 7–10 am local time) and the afternoon (1–4 pm; Figure 13). The mass spectrum of the morning organic aerosols shows prominent peaks at *m/z* 55 ($C_4H_7^+$ and $C_3H_3O^+$) and 57 ($C_4H_9^+$), which are generally associated with primary (combustion-emitted) organics from combustion sources [*Alfarra et al.*, 2004; *Canagaratna et al.*, 2004], while that of the afternoon organic aerosols is dominated by *m/z* 44 (CO_2^+), which is a pronounced peak in the AMS mass spectra of oxygenated organics [*Alfarra et al.*, 2004; *Drewnick et al.*, 2004b]. Note that *m/z* 43 ($C_3H_7^+$ and $C_2H_3O^+$) is a major peak in both mass spectra, because it is produced in roughly equal fractions from primary and secondary/oxidized organic aerosols and therefore is more of a surrogate for the bulk organics. In addition, mass fragments that are representative for combustion source organic species, such as *m/z* 69, 71, 85, 91 and 95 [*McLafferty and Turecek*, 1993], are all comparatively higher in the mass spectrum of the morning organics (Figure 13). Overall these mass spectra are consistent with morning organic aerosols having a higher contribution of traffic-related combustion source emissions while the afternoon aerosols appear to be more oxidized.

[58] A study with two AMSs at 3 sites in the Vancouver area in Canada reported much more marked differences between the mass spectra of urban and rural organic aerosols [*Alfarra et al.*, 2004] than between the morning and afternoon spectra in this study. The reason for the relatively smaller difference in the mass spectra in this study is that primary aerosols always contribute to the observed concentrations in Pittsburgh, while their contribution is very small for the rural aerosol in Vancouver. In addition, relatively high background of oxidized organic aerosols has been observed in both studies most of the time.

[59] Since aged organic species more likely reside in the accumulation mode, we compared the diurnal profiles of small mode (D_{va} = 30–100 nm) and accumulation mode (D_{va} = 250–1000 nm) organics (Figure 14). The mass concentrations of the ultrafine mode are elevated in the morning and evening rush hours and are much lower in the afternoon when photochemistry is usually intense. The accumulation mode on the other hand, did not show much of a diurnal variation. The average mass loading of the accumulation mode organic aerosols increased slightly between 1 pm and 4 pm, suggesting the formation of secondary organic aerosols. We observed a comparatively good correlation between the accumulation mode organics and sulfate (r^2 = 0.73; Figure 15), which is an indication that these two species are likely internally mixed in the accumulation mode particles. The slope of the regression

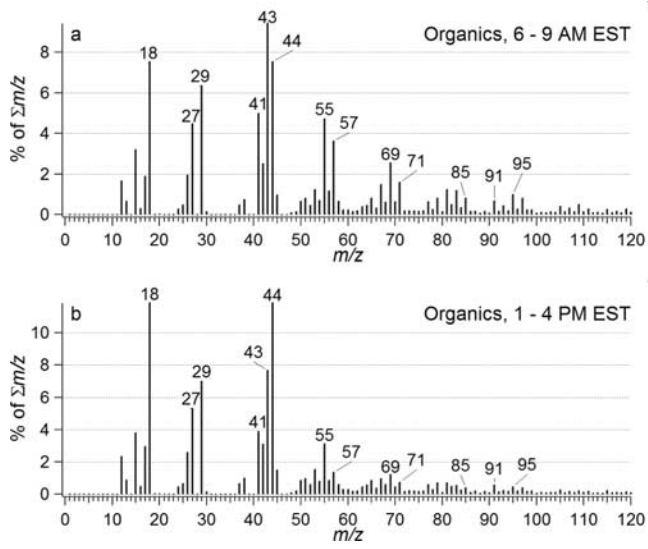

Figure 13. Average AMS mass spectra of organic particles during (a) 6–9 am and (b) 1–4 pm (7–22 September 2002 EST). Note that local time during this study was EDT, which is 1 hour ahead of EST.

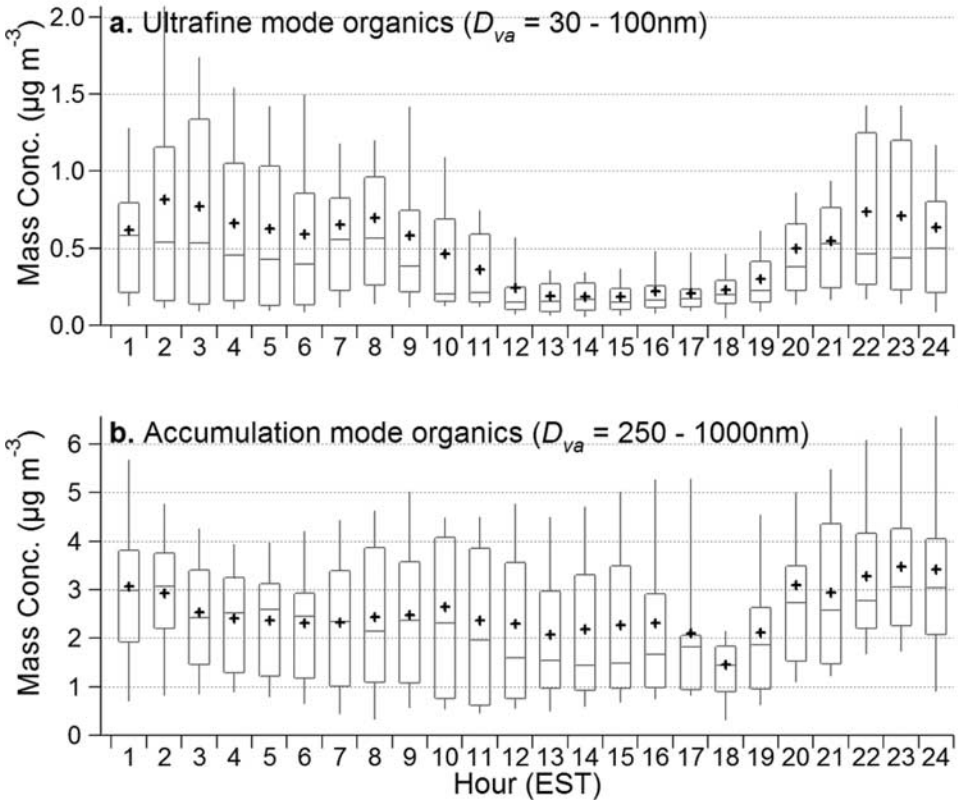

Figure 14. Average diurnal variations of (a) the ultrafine and (b) the accumulation mode organic particles during 7–22 September 2002 EST.

line likely represents the ratio of the source strengths of both aerosol types in the region.

4. Conclusions

[60] Nonrefractory submicron particles (NR-PM_1) were measured in Pittsburgh from 7 to 22 September 2002 using an Aerodyne AMS. Reasonably good agreement was observed between the AMS and collocated instruments on total and species mass concentrations, and on size distributions, with smaller AMS concentrations likely due to the difference between PM_1 and $PM_{2.5}$. The comparisons of the size distributions obtained by the AMS and the SPMS, and the AMS composition data suggest that the average density of particles in Pittsburgh during this period was ~1.5 g cm^{-3}.

[61] Submicron particles in Pittsburgh during this time period were generally characterized by high contents of SO_4^{2-} and organics, and low levels of NO_3^- and Cl^-. The mass balance between NH_4^+ and the anions suggest that the majority of the particles are neutralized to slightly acidic. However, during relatively polluted periods significantly acidic particles (i.e., those estimated to contain approximately equal or larger amounts of NH_4HSO_4 than $(NH_4)_2SO_4$) are observed. Compared to neutralized particles, acidic particles generally contain significantly more sulfate, comparable amounts of organics and NH_4^+, and less NO_3^- and Cl^-. We see no evidence of enhanced secondary organic aerosol formation due to acid-catalyzed organic chemistry.

[62] We observed a quickly changing aerosol population due to the combined influences from transport, local emissions, gas-to-particle conversion, and photochemistry. Through this entire study, the mass concentration of NR-PM_1 varies from below 1 μg m^{-3} to as high as ~70 μg m^{-3}, with an average value of ~15 μg m^{-3} and a

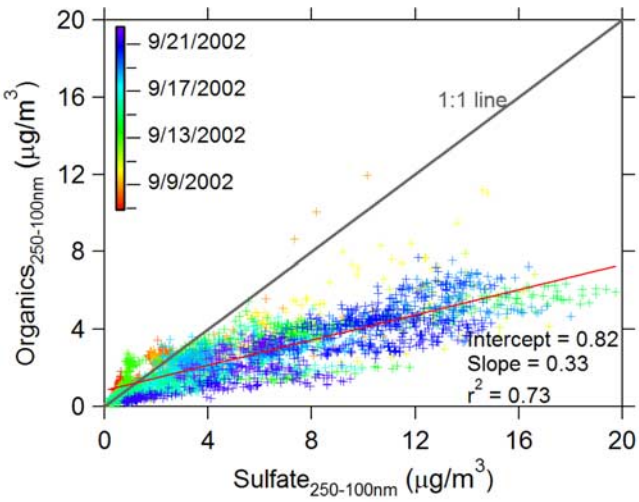

Figure 15. Correlation between organics and sulfate in the D_{va} = 250–1500 nm particles. Data points are colored by the time. The red line is a linear fit to the data.

standard deviation of 9 μg m^{-3}. The mass concentrations and size distributions of particulate species vary on timescales between less than an hour to ~2 days. On the basis of the size distributions and diurnal profiles of the particle species, in addition to the mass spectra of the organic aerosols, we found that the NR-PM_1 particles in Pittsburgh are composed of 3 major modes, an ultrafine mode that is mainly composed of traffic organics, a relatively aged mode that likely grew by gaseous condensation, and an accumulation mode that is dominated by sulfate and ammonium.

Appendix A: Removal of Gaseous Interference From the Size Distribution of Ammonium

[63] The NH_4^+ size distribution was derived from the signal distribution of *m/z* 16 (NH_2^+) in the P-TOF range corresponding to the sizes of the particles transmitted into the AMS. However, the O^+ (also *m/z* 16) signal from the ionization of gas phase O_2 tails into the particle region, interfering with the measurement of NH_4^+ in small particles for D_{va} < 100 nm (Figure A1). The tail of the O_2 signal, which is attributed to a spread in the velocities of O_2 molecules after the focusing lens, can be modeled using an exponential fit that has the same functional form as the one-dimensional Boltzmann velocity distribution function [*Atkins*, 1998; *Morris*, 2002],

$$s = a \times \exp\left(-\frac{(v-b)^2}{c}\right) \quad \text{(A1)}$$

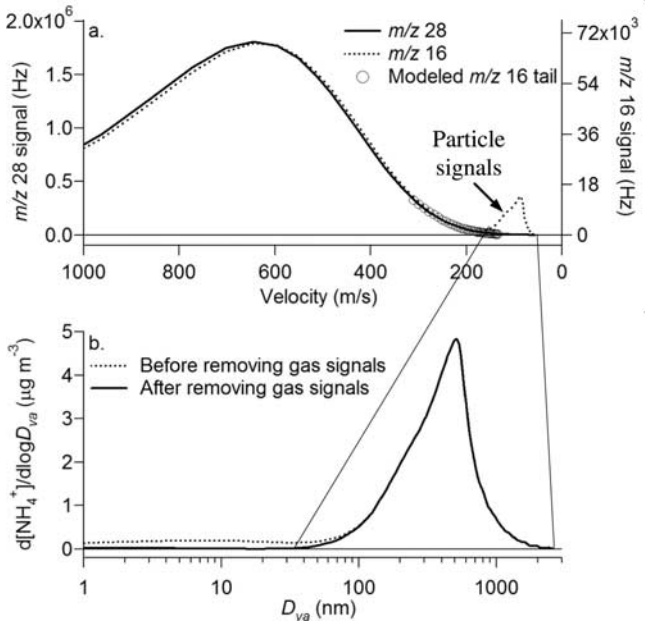

Figure A1. (a) Distributions of *m/z* 16 (NH_2^+ and O^+) and 28 (N_2^+) signals as a function of measured particle velocity; (b) mass distributions of ammonium as a function of D_{va} before and after the removal of gas phase O^+ signals.

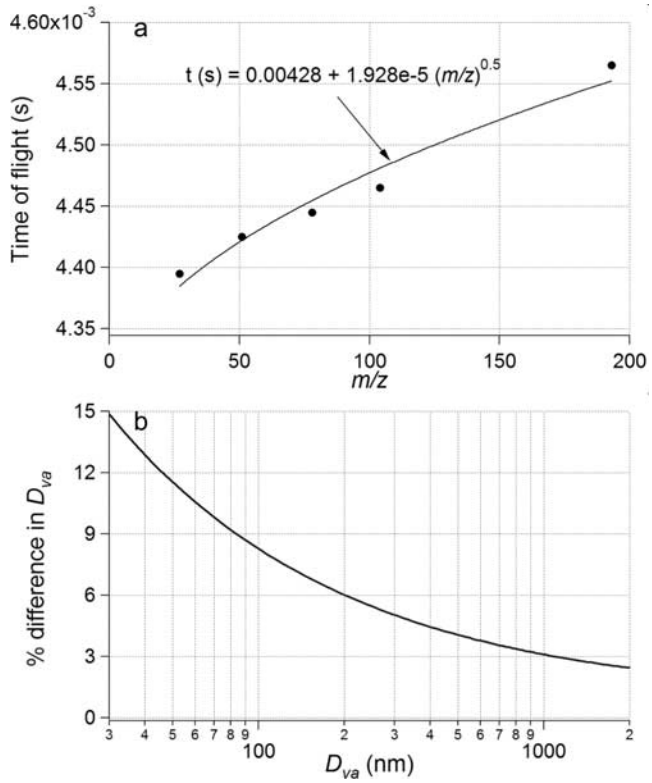

Figure B1. (a) P-TOF of ions (*m/z* = 27, 51, 78, 104 and 193; quadrupole extraction voltage = 180 V) originated from monodisperse 500 nm PSL spheres; (b) differences in D_{va} due to 60 μs difference in P-TOF plotted as a function of particle size.

where *s* is the ion rate (Hz) detected for the signal, *a*, *b*, and *c* are fit parameters, and *v* is the velocity of the species measured in the P-TOF sizing chamber.

[64] Because the same function should apply to all gaseous species, N_2 and O_2 alike, we estimated the *a*, *b*, and *c* values by fitting the signal distribution of *m/z* 28 (N_2^+) to equation (A1), for P-TOFs corresponding to 1–200 nm in D_{va} (Figure A1a). *m/z* 28 was chosen because among all *m/z* it has the highest signal-to-noise ratio and is the least affected by particle signals. Using the fitted *a*, *b*, and *c* values, the gas phase signals of *m/z* 16 were then calculated and subtracted from the 1–200 nm region to give "filtered" NH_4^+ distributions (Figure A1a). All reported size distributions of NH_4^+ were corrected with this method. It needs to be noted that this correction is negligible for particles larger than D_{va} of ~70 nm (Figure A1b), but is critical for a quantitative examination of the chemistry of new particles during the nucleation events [*Zhang et al.*, 2004].

[65] The same technique is generally applicable to removal of gas signals from the size distributions of particle species, such as *m/z* 28 (CO^+) and *m/z* 44 (CO_2^+) for organics and 18 (H_2O^+) for water. At ambient conditions, except for *m/z* 28, whose size distribution in the particle range is hugely influenced by gaseous N_2, other *m/z* generally chosen in P-TOF mode contain negligible amounts of gas signals compared to the particle signals because the aerodynamic lens and skimmers of

the AMS reduce the concentration of gas phase species by a factor of 10^7 relative to aerosol species [*Allan et al.*, 2004b].

Appendix B: Adjustment of the NH_4^+ Size Distributions for Faster Ion Flight in the Quadrupole

[66] We observed a small (approximately 60 μs) shift in time of flight between the distributions of ammonium and sulfate throughout this campaign. The shift arises partly because the NH_2^+ ion (*m*/*z* 16) travels slightly faster within the quadrupole than the SO^+ and SO_2^+ ions (*m*/*z* 48 and 64) do. This is expected since all singly charged ions have the same kinetic energy of about 14 eV in the quadrupole (as used in AMS instruments), and thus the dwelling times of ions in the quadrupole are proportional to the square root of the mass to charge ratio of the ions. To adjust for this mass-dependent ion transition time in the quadrupole we measured the apparent P-TOF for various PSL ions originated from the same monodisperse particles. This experiment shows that the average difference between the P-TOFs of SO_4^{2-} ions and that of NH_4^+ was indeed ~60 μs (Figure B1). Because no obvious shifts in P-TOF were observed between internally mixed SO_4^{2-} and NO_3^- or organics we adjusted the size distributions of NH_4^+ by increasing its time of flight by 60 μs.

[67] As shown in Figure B1b, the relationship between D_{va} and P-TOF is nonlinear: a 60 μs difference in P-TOF translates into ~10–15% difference in D_{va} in particles smaller than 70 nm but only 4–5% for the accumulation mode particles. As such, this is most important for the small size NH_4^+, which is only significant during the new particle formation and growth events [*Zhang et al.*, 2004].

[68] **Acknowledgments.** The authors thank Spyros Pandis (CMU) for organizing and directing the PAQS campaign and inviting us to participate in the study, Beth Wittig (CMU) for TEOM, continuous sulfate, gas phase and meteorological data, Charles Stanier (CMU) for particle number distribution data, R. Subramanian (CMU), Allen Robinson (CMU), Andrea Polidori (Rutgers University), and Barbara Turpin (Rutgers University) for OC data, Juan Cabada (CMU) for MOUDI data, Andrey Khlystov (CMU) for ammonium data and logistical assistance during this study, and James Allan (UMIST), Frank Drewnick (Max Planck Institute for Chemistry), and Alice Delia (CU) for AMS data analysis software. We also thank an anonymous reviewer for useful comments that helped us improve the manuscript. This research was conducted as part of the Pittsburgh Air Quality Study and was supported by the University of Colorado through J. L. Jimenez's Startup Fund.

References

Alfarra, M. R., et al. (2004), Characterization of urban and regional organic aerosols in the lower Fraser Valley using two Aerodyne aerosol mass spectrometers, *Atmos. Environ.*, *38*, 5745–5758.

Allan, J. D., et al. (2003a), Quantitative sampling using an Aerodyne aerosol mass spectrometer: 2. Measurements of fine particulate chemical composition in two UK cities, *J. Geophys. Res.*, *108*(D3), 4091, doi:10.1029/2002JD002359.

Allan, J. D., J. L. Jimenez, P. I. Williams, M. R. Alfarra, K. N. Bower, J. T. Jayne, H. Coe, and D. R. Worsnop (2003b), Quantitative sampling using an Aerodyne aerosol mass spectrometer: 1. Techniques of data interpretation and error analysis, *J. Geophys. Res.*, *108*(D3), 4090, doi:10.1029/2002JD002358.

Allan, J. D., et al. (2004a), Submicron aerosol composition at Trinidad Head, California, during ITCT 2K2: Its relationship with gas phase volatile organic carbon and assessment of instrument performance, *J. Geophys. Res.*, *109*(D23), D23S24, doi:10.1029/2003JD004208.

Allan, J. D., et al. (2004b), A generalised method for the extraction of chemically resolved mass spectra from Aerodyne aerosol mass spectrometer data, *J. Aerosol Sci.*, *35*(7), 909–922 doi:10.1016/j.jaerosci.2004.02.007.

Anderson, R. R., D. V. Martello, C. M. White, K. C. Crist, K. John, W. K. Modey, and D. J. Eatough (2004), The regional nature of $PM_{2.5}$ episodes in the upper Ohio river valley, *Air Waste Manage. Assoc.*, *54*, 971–984.

Atkins, P. W. (1998), *Physical Chemistry*, Oxford Univ. Press, New York.

Bahreini, R., J. L. Jimenez, J. Wang, R. C. Flagan, J. H. Seinfeld, J. T. Jayne, and D. R. Worsnop (2003), Aircraft-based aerosol size and composition measurements during ACE-Asia using an Aerodyne aerosol mass spectrometer, *J. Geophys. Res.*, *108*(D23), 8645, doi:10.1029/2002JD003226.

Bein, K. J., Y. Zhao, A. S. Wexler, and M. V. Johnston (2005), Speciation of size-resolved individual ultrafine particles in Pittsburgh, Pennsylvania, *J. Geophys. Res.*, *110*, D07S05, doi:10.1029/2004JD004708, in press.

Boudries, H., et al. (2004), Chemical and physical processes controlling the distribution of aerosols in the lower Fraser Valley, Canada, during the PACIFIC 2001 field campaign, *Atmos. Environ.*, *38*, 5759–5774.

Brown, S. S., H. Stark, and A. R. Ravishankara (2003a), Applicability of the steady state approximation to the interpretation of atmospheric observations of NO_3 and N_2O_5, *J. Geophys. Res.*, *108*(D17), 4539, doi:10.1029/2003JD003407.

Brown, S. S., H. Stark, T. B. Ryerson, E. J. Williams, D. K. Nicks Jr., M. Trainer, F. C. Fehsenfeld, and A. R. Ravishankara (2003b), Nitrogen oxides in the nocturnal boundary layer: Simultaneous in situ measurements of NO_3, N_2O_5, NO_2, NO, and O_3, *J. Geophys. Res.*, *108*(D9), 4299, doi:10.1029/2002JD002917.

Bytnerowicz, A., and M. E. Fenn (1996), Nitrogen deposition in California forests: A review, *Environ. Pollut.*, *92*(2), 127–146.

Cabada, J. C., S. N. Pandis, and A. L. Robinson (2002), Sources of atmospheric carbonaceous particulate matter in Pittsburgh, Pennsylvania, *J. Air Waste Manage. Assoc.*, *52*(6), 732–741.

Cabada, J. C., S. Rees, S. Takahama, A. Khlystov, S. N. Pandis, C. I. Davidson, and A. L. Robinson (2004), Mass size distributions and size resolved chemical composition of fine particulate matter at the Pittsburgh Supersite, *Atmos. Environ.*, *38*, 3127–3141.

Canagaratna, M. R., et al. (2004), Chase studies of particulate emissions from in-use New York city vehicles, *Aerosol Sci. Technol.*, *38*, 555–573, doi:10.1080/02786820490465504.

DeCarlo, P., J. G. Slowik, D. R. Worsnop, P. Davidovits, and J. L. Jimenez (2004), Particle morphology and density characterization by combined mobility and aerodynamic diameter measurements. Part 1: Theory, *Aerosol Sci. Technol.*, *38*, 1185–1205, doi:10.1080/02786829093907.

Dockery, D. W., C. A. Pope, X. P. Xu, J. D. Spengler, J. H. Ware, M. E. Fay, B. G. Ferris, and F. E. Speizer (1993), An association between air pollution and mortality in 6 United States cities, *N. Engl. J. Med.*, *329*(24), 1753–1759.

Drewnick, F., J. J. Schwab, O. Hogrefe, S. Peters, L. Husain, D. Diamond, R. Weber, and K. L. Demerjian (2004a), Intercomparison and evaluation of four semi-continuous $PM_{2.5}$ sulfate instruments, *Atmos. Environ.*, *37*(24), 3335–3350.

Drewnick, F., J. J. Schwab, J. T. Jayne, M. Canagaratna, D. R. Worsnop, and K. L. Demerjian (2004b), Measurement of ambient aerosol composition during the PMTACS-NY 2001 using an aerosol mass spectrometer. Part I: Mass concentrations, *Aerosol Sci. Technol.*, *38*, suppl. 1, 92–103.

Drewnick, F., J. J. Schwab, J. T. Jayne, M. Canagaratna, D. R. Worsnop, and K. L. Demerjian (2004c), Measurement of ambient aerosol composition during the PMTACS-NY 2001 using an aerosol mass spectrometer. Part II: Chemically speciated mass distributions, *Aerosol Sci. Technol.*, *38*, suppl. 1, 104–117.

Heberlein, J., et al. (2001), Thermal plasma deposition of nanophase hard coatings, *Surface Coatings Technol.*, *142*, 265–271.

Intergovernmental Panel on Climate Change (IPCC) (2001), *Climate Change 2001: The Scientific Basis, Contribution of Working Group I to the Third Assessment Report of the Intergovernmental Panel on Climate Change*, edited by J. T. Houghton et al., Cambridge Univ. Press, New York.

Jang, M. S., N. M. Czoschke, S. Lee, and R. M. Kamens (2002), Heterogeneous atmospheric aerosol production by acid-catalyzed particle-phase reactions, *Science*, *298*(5594), 814–817.

Jayne, J. T., D. C. Leard, X. Zhang, P. Davidovits, K. A. Smith, C. E. Kolb, and D. R. Worsnop (2000), Development of an aerosol mass spectrometer for size and composition analysis of submicron particles, *Aerosol Sci. Technol.*, *33*, 49–70.

Jimenez, J. L., R. Bahreini, D. R. Cocker, H. Zhuang, V. Varutbangkul, R. C. Flagan, J. H. Seinfeld, C. O'Dowd, and T. Hoffmann (2003a), Correction to "New particle formation from photooxidation of diiodomethane (CH_2I_2)," *J. Geophys. Res.*, *108*(D23), 4733, doi:10.1029/2003JD004249.

Jimenez, J. L., R. Bahreini, D. R. Cocker, H. Zhuang, V. Varutbangkul, R. C. Flagan, J. H. Seinfeld, C. O'Dowd, and T. Hoffmann (2003b), New particle formation from photooxidation of diiodomethane (CH_2I_2), *J. Geophys. Res.*, *108*(D10), 4318, doi:10.1029/2002JD002452.

Jimenez, J. L., et al. (2003c), Ambient aerosol sampling with an aerosol mass spectrometer, *J. Geophys. Res.*, *108*(D7), 8425, doi:10.1029/2001JD001213.

Khlystov, A., G. P. Wyers, and J. Slanina (1995), The steam-jet aerosol collector, *Atmos. Environ.*, *29*(17), 2229–2234.

Khlystov, A. Y., B. Wittig, and C. Davidson (2001), Quality Assurance Project Plan for the Pittsburgh Air Quality Study, U.S. Environ. Prot. Agency, Research Triangle Park, N. C.

Lee, S., D. M. Murphy, D. S. Thomson, and A. M. Middlebrook (2003), Nitrate and oxidized organic ions in single particle mass spectra during the 1999 Atlanta Supersite Project, *J. Geophys. Res.*, *108*(D7), 8417, doi:10.1029/2001JD001455.

McLafferty, F. W., and F. Turecek (1993), *Interpretation of Mass Spectra*, Univ. Sci. Books, Mill Valley, Calif.

McMurry, P. H. (2000), A review of atmospheric aerosol measurements, *Atmos. Environ.*, *34*(12–14), 1959–1999.

Middlebrook, A., et al. (2003), An intercomparison of particle mass spectrometers during the 1999 Atlanta Supersite Project, *J. Geophys. Res.*, *108*(D7), 8424, doi:10.1029/2001JD000660.

Morris, J. W. (2002), Chemical kinetics and microphysics of atmospheric aerosols, Ph.D. thesis, Boston Coll., Boston, Mass.

Morris, J. W., P. Davidovits, J. T. Jayne, J. L. Jimenez, Q. Shi, C. E. Kolb, D. R. Worsnop, W. S. Barney, and G. Cass (2002), Kinetics of submicron oleic acid aerosols with ozone: A novel aerosol mass spectrometric technique, *Geophys. Res. Lett.*, *29*(9), 1357, doi:10.1029/2002GL014692.

Murphy, D. M., D. S. Thomson, and T. M. J. Mahoney (1998), In situ measurements of organics, meteoritic material, mercury, and other elements in aerosols at 5 to 19 kilometers, *Science*, *282*(5394), 1664–1669.

Paerl, H. W., C. Aguilar, and M. L. Fogel (1997), Atmospheric nitrogen deposition in estuarine and coastal waters: Biogeochemical and water quality impacts, in *Atmospheric Deposition of Contaminants to the Great Lakes and Coastal Waters*, edited by J. E. Baker, pp. 415–429, SETAC Press, Pensacola, Fla.

Pandis, S. N., A. S. Wexler, and J. H. Seinfeld (1995), Dynamics of tropospheric aerosols, *J. Physical Chemistry*, *99*(24), 9646–9659.

Park, K., D. B. Kittelson, M. R. Zachariah, and P. H. McMurry (2004), Measurement of inherent material density of nanoparticle agglomerates, *J. Nanoparticle Res.*, *6*(2), 267–272.

Pope, C. A., R. T. Burnett, M. J. Thun, E. E. Calle, D. Krewski, K. Ito, and G. D. Thurston (2002), Lung cancer, cardiopulmonary mortality, and long-term exposure to fine particulate air pollution, *J. Am. Med. Assoc.*, *287*(9), 1132–1141.

Rees, S. L., A. L. Robinson, A. Khlystov, C. O. Stanier, and S. N. Pandis (2004), Mass balance closure and the Federal Reference Method for $PM_{2.5}$ in Pittsburgh, Pennsylvania, *Atmos. Environ.*, *28*(20), 3305–3318.

Russell, L. M. (2003), Aerosol organic-mass-to-organic-carbon ratio measurements, *Environ. Sci. Technol.*, *37*(13), 2982–2987.

Schindler, D. W. (1988), Effects of acid-rain on fresh-water ecosystems, *Science*, *239*(4836), 149–157.

Seinfeld, J. H., and S. N. Pandis (1998), *Atmospheric Chemistry and Physics: From Air Pollution to Climate Change*, 1326 pp., John Wiley, Hoboken, N. J.

Slowik, J. G., K. Stainken, P. Davidovits, L. R. Williams, J. T. Jayne, C. E. Kolb, D. R. Worsnop, Y. Rudich, P. DeCarlo, and J. L. Jimenez (2004), Particle morphology and density characterization by combined mobility and aerodynamic diameter measurements. Part 2: Application to combustion generated soot particles as a function of fuel equivalence ratio, *Aerosol Sci. Technol.*, *38*, 1206–1222, doi:10.1080/027868290903916.

Solomon, S. (1999), Stratospheric ozone depletion: A review of concepts and history, *Rev. Geophys.*, *37*(3), 275–316.

Stanier, C., A. Khlystov, and S. Pandis (2004), Nucleation events during the Pittsburgh Air Quality Study: Description and relation to key meteorological, gas phase, and aerosol parameters, *Aerosol Sci. Technol.*, *38*, suppl. 1, 253–264.

Stolzenburg, M., and S. V. Hering (2003), Method for the automated measurement of fine particle nitrate in the atmosphere, *Environ. Sci. Technol.*, *34*, 907–914.

Subramanian, R., A. Y. Khlystov, J. C. Cabada, and A. L. Robinson (2004), Positive and negative artifacts in particulate organic carbon measurements with denuded and undenuded sampler configurations, *Aerosol Sci. Technol.*, *38*, suppl. 1, 27–48.

Suess, D. T., and K. A. Prather (1999), Mass spectrometry of aerosols, *Chem. Rev.*, *99*(10), 3007–3035.

Tang, W., T. Raymond, B. Wittig, C. Davidson, S. Pandis, A. Robinson, and K. Crist (2004), Spatial variations of $PM_{2.5}$ during the Pittsburgh Air Quality Study, *Aerosol Sci. Technol.*, *38*, suppl. 2, 80–90.

Tobias, H. J., P. M. Kooiman, K. S. Docherty, and P. J. Ziemann (2000), Real-time chemical analysis of organic aerosols using a thermal desorption particle beam mass spectrometer, *Aerosol Sci. Technol.*, *33*(1–2), 170–190.

Turpin, B. J., and H. J. Lim (2001), Species contributions to $PM_{2.5}$ mass concentrations: Revisiting common assumptions for estimating organic mass, *Aerosol Sci. Technol.*, *35*(1), 602–610.

Turpin, B. J., R. A. Cary, and J. J. Huntzicker (1990), An in-situ time-resolved analyzer for aerosol organic and elemental carbon, *Aerosol Sci. Technol.*, *12*, 161–171.

Watson, J. G. (2002), Visibility: Science and regulation, *J. Air Waste Manage. Assoc.*, *52*(6), 628–713.

West, J. J., A. S. Ansari, and S. N. Pandis (1999), Marginal $PM_{2.5}$: Nonlinear aerosol mass response to sulfate reductions in the eastern United States, *J. Air Waste Manage. Assoc.*, *49*(12), 1415–1424.

Wittig, A. E., N. Anderson, A. Y. Khlystov, S. N. Pandis, C. Davidson, and A. L. Robinson (2004), Pittsburgh Air Quality Study overview and initial scientific findings, *Atmos. Environ.*, *38*, 3107–3125.

Zhang, Q., C. O. Stanier, M. R. Canagaratna, J. T. Jayne, D. R. Worsnop, S. N. Pandis, and J. L. Jimenez (2004), Insights into the chemistry of new particle formation and growth events in Pittsburgh based on aerosol mass spectrometry, *Environ. Sci. Technol.*, *38*(18), 4797–4809, doi:10.1021/es035417u.

M. R. Canagaratna, J. T. Jayne, and D. R. Worsnop, Aerodyne Research Inc., Billerica, MA 01821-3976, USA.

J.-L. Jimenez and Q. Zhang, Cooperative Institute for Research in Environmental Sciences (CIRES), University of Colorado, Boulder, 216 UCB, Boulder, CO 80309-0216, USA. (jose.jimenez@colorado.edu; zhangq@cires.colorado.edu)